U.S. DEPARTMENT OF COMMERCE
NATIONAL OCEANIC AND ATMOSPHERIC ADMINISTRATION
NATIONAL WEATHER SERVICE
NATIONAL METEOROLOGICAL CENTER

OFFICE NOTE 362

GLOBAL FORECAST-ERROR CORRELATION, PART 1: ISOBARIC WIND AND GEOPOTENTIAL

H. JEAN THIEBAUX, LAUREN L. MORONE AND RICHARD L. WOBUS

OCTOBER 1989

GLOBAL FORECAST-ERROR CORRELATION, PART 1: ISOBARIC WIND AND GEOPOTENTIAL

H. Jean Thiebaux, Lauren L. Morone and Richard L. Wobus

NOAA/NWS/NMC2, Washington D.C. 20233

ABSTRACT

Results of a thorough study of the correlation structure of observation-minus-forecast increments for mandatory pressure level radiosonde observations of zonal and meridional wind components and geopotential, differenced with NMC's 6-hour global forecasts, are reported. Our work focused on the selection of a representation for spatial lag-correlations to be used in updating the multivariate statistical objective analysis algorithm of the global data assimilation system, with attention given to regional and seasonal dependence of the correlation structure, and on the degree to which the increments are in the same geostrophic balance as the signal and forecast fields individually.

We compare the performance of several candidates for representing geopotential autocorrelations, on the one hand, and the auto- and cross-correlations of the wind components, on the other, for five mandatory pressure levels, for four regions of the Northern Hemisphere and for the Southern Hemisphere; and we identify one functional form as optimal for global objective analysis. The parameters are shown to vary with level and season. Furthermore, the geopotential and wind correlation fits have identified important differences in corresponding parameter values.

A single algorithm which covers the primary candidates in one fitting operation, for future semi-automatic updating, has been developed in the course of this work. Results of its use are presented and discussed. Part 2 will add the vertical component of three-dimensional correlation structure, and present analysis and forecast impact test results of use of this structure in the global optimal interpolation algorithm.

1. Introduction

A detailed study of the correlation structure of observation-minus-forecast differences of mandatory level winds and heights has recently been completed at the U. S. National Meteorological Center (NMC). The two-fold objective for this was a major update of the wind and height forecast-error correlation representations used in NMC's global data assimilation system and the creation of a routine re-parameterization algorithm. We have achieved this; and the scope of the data included in our study has clearly identified a requirement for updating, to keep pace with seasonal changes in the observed fields and with changes in f.e. correlation structure brought through continual advances in the NMC's NWP models.

The work we report here is a global study of isobaric correlation structure of RAOB-minus-(6 hour) forecast differences for NMC's global spectral model. In addition to seeking to establish the best functional form to represent spatial correlation properties of these forecast variable increments we addressed correlation parameter questions pertaining to

a) geopotential structure, namely,
   - i) regional (dis)similarities,
   - ii) latitude dependencies, within continental regions,
   - iii) variations with pressure, in the vertical,
   - iv) differences between seasons,

and

b) wind f.e. structure, principally the question of whether the geostrophic assumption applied to forecast errors carries through to provide the optimal parameterization for correlations of the wind increments.

In addition to these preset goals, our work provided additional significant insights regarding marked change in f.e. correlation structure with change in the forecast model, and the impact of computing and removing an estimate of the systematic error of the forecast cycle.

Bergman (1979) had primary responsibility for the formulation of the multivariate analysis scheme which has been basic to NMC's global data assimilation system and which, for a number of years, served as a model for objective analysis of observation-minus-forecast increments at major forecast centers of the World. Bergman's scheme was based on the use of the negative-squared-exponential function* $\exp(-b\tau^2)$ to represent isobaric temperature, and later geopotential, f.e. correlation as a function of separation between locations. Auto- and cross-correlations for wind component f.e.s were derived from this function by assuming that the forecast errors of U and V are geostrophically related to geopotential f.e. increments.

---

*Bergman and others referred to this as the "Gaussian correlation function" because of its similarity to the density function of K. F. Gauss' error distribution curve.

During the past few years other forecast centers have developed alternate models for f.e. correlations, which have provided improved fits to their indigenous multivariate correlation structures. For example, see Hollingsworth and Lonnberg (1986) for the ECMWF, Lorenc (1988) for the U.K. Met.Office, Goerss (1989) for the US/NEPRF, and Thiebaux, Mitchell and Shantz (1987) for RPN and the CMC. The basic functional representations for geopotential f.e.s considered to best fit the differences between radiosonde derived observations (RAOBs) and the forecasts made by these centers are, respectively:

isotropic Fourier-Bessel series,

second-order autoregressive correlation function,

exponentially-damped cosine.

The ANMRC is introducing a new statistical objective analysis scheme using a negative-squared-exponential correlation model (Bourke, et al, 1989).

Candidate representations for geopotential f.e. correlations, in our study, included the correlation functions of low order autoregressive processes in addition to the traditional negative-squared-exponential representation and two, low order, inverse polynomials. Auto- and cross-correlation function candidates for wind f.e.s were all derived from the basis representation for geopotential f.e. correlation, by assuming that the wind component f.e.s are geostrophic. The criterion for selection from the candidates, of a "best" representation

for wind and geopotential f.e. correlations, is minimization of the root-mean-square-differences (RMSDs) with correlations of RAOB-minus-(6 hour) forecast differences computed from the observations and forecasts of a full season.

Section 2 presents candidate functions for geopotential f.e. correlation and the basis functions for f.e. correlations of the wind fields, with properties relevant to their use in multivariate objective analysis. Section 3 describes our reference data sets, with the criteria used their construction, and our rationale for choice of regional subdivisions for geographic comparisons; and it discusses simultaneous fitting of the five, wind field, f.e. correlation arrays, with our suite of candidate correlation models. Section 4 establishes the optimal representation for height/height correlations. (The outcome is surprising, although fully consistent with NWP improvements in recent years). Regional, and latitude and pressure level dependencies of correlation function parameters are described. Section 4 also describes the results of fitting sets of geostrophic wind correlation functions to observed correlation arrays for the forecast errors of the wind components. Section 5 concludes our report with an overview of our study, and it s implications for present and future analysis algorithm updating.

The present paper confines attention to representation of correlation structures on constant pressure surfaces.

Operational objective analysis requires specification of three-dimensional correlations of the observation-minus-forecast increments of wind components and geopotential. Representation of the vertical factors which, in combination with the isobaric correlation functions, describe the full three-dimensional structure, will be addressed in Part 2.

2. Candidate representations for isobaric correlation structure

This section describes the set of correlation models considered as candidates for geopotential, forecast-minus-observation differences (f.e.s), with the rationale for our choices. It then devotes primary attention to derivation of auto- and cross-correlation models for the f.e.s of the wind field, by imposing geostrophic constraints on U- and V-wind f.e.s, and focusing on required properties of candidate correlation basis functions. Here "candidate correlation basis function" refers to a correlation model for isobaric height f.e.s, from which auto- and cross-correlation models for wind component f.e.s are derived by assuming the wind f.e.s are geostrophically related to geopotential f.e.s.

The forms of the models of isobaric spatial correlation structure, which are compared for their capacities to represent observed f.e. correlations as functions of location separation, fall into four categories -- on the basis of rationale for inclusion:

Category I. is comprised of the classic correlation model for forecast-minus-observation differences of both geopotential and temperature (Bergman, 1979; Burke, et al, 1989; Rutherford, 1972; Schlatter, 1975):

$$R(r) = \exp(-br^2)$$

which we refer to as the "negative squared exponential" and abbreviate SQEX.

Category II. is comprised of a family of functions, the members of which are derived from stochastic autoregressive representations of geopotential f.e.s, or "increments". That is, at any given time, the increment field is regarded as the state of a spatially coherent, time evolutionary stochastic/dynamic process. The theoretical assumptions made in these derivations are that the discrepancies between (6-hour) forecast and reported geopotential values, have zero ensemble means and are regionally, second order stationary. Mathematical details of the derivations of these functions from representations of the forecast error field as the output of a linear filter driven by white noise, are given in Thiebaux and Pedder (1987), with references to experiments with these models which have been reported in the meteorological literature. The geopotential f.e. correlation functions in this category are as follows:

i) The correlation function for an isotropic, first-order autoregressive process

$$R(\tau) = \exp(-b\tau), \qquad \tau > 0$$

which is the well-known negative exponential function and will be abbreviated FOAR, for "first order autoregressive".

ii) The correlation function for an isotopic second-order autoregressive process

$$R(\tau) = \left[\cos(a\tau) + \frac{c}{a}\sin(a\tau)\right]\exp(-c\tau), \quad \tau > 0,$$

for which we will use the designation SOAR.

iii) The correlation function for an isotropic third-order autoregressive process

$$R(\tau) = \left[\alpha\cos(b\tau) + \beta\sin(b\tau)\right]\exp(-a\tau) + \gamma\exp(-c\tau),$$

$$\tau > 0 \quad \text{and} \quad (\alpha, \beta, \gamma) = \underset{\sim}{g}(a, b, c),$$

which will be designated TOAR.

iv) The correlation function for an anisotropic second-order autoregressive process

$$R(\Delta\phi, \Delta\lambda) = \prod_{j=1}^{2}\left[\cos(a_j\tau_j) + \frac{c_j}{a_j}\sin(a_j\tau_j)\right]\exp(-c_j\tau_j),$$

$$\tau_1 = \Delta\phi > 0 \quad \text{and} \quad \tau_2 = \Delta\lambda > 0.$$

Category III. is a small family, of two functions which are reciprocals of low-order polynomials:

$$R(\tau) = (1 + a\tau^2 + b\tau^4 + c\tau^6)^{-1}$$

and

$$R(\tau) = (1 + a\tau^2 + b\tau^4 + c\tau^6 + d\tau^8 + e\tau^{10})^{-1}.$$

This category was included with the expectation that increasing the number of adjustable parameters in the function used to represent the location-separation dependence of f.e.

correlations would increase the goodness-of-fit of the function to observed correlation structure. Category IV. has one member, suggested by Gandin (1988):

$$R(r) = \left(1 + ar + \frac{(ar)^2}{3}\right) \exp(-ar)$$

which we refer to as Kagan's function.

One of the functions identified above does not satisfy requirements for candidate correlation basis functions, as enumerated in Julian and Thiebaux (1975), for example. This function is the FOAR. We include it among the functions fit to arrays of auto-correlations of geopotential f.e.s; although it is necessarily excluded from consideration in relation to wind f.e.s.

In the derivation of correlation representations for f.e.s of the wind components, namely for

U,U V,V U,V U,Z and V,Z

we write the covariance for geopotential f.e.s as

$$\mathcal{C}(Z,Z) = \sigma_Z^2 R(r)$$

where σ_Z^2 signifies variance and $R(r)$ the geopotential f.e. correlation basis function. r denotes the separation between locations of observed or analyzed geopotential values, and is always taken to be positive. The assumed geostrophic relations among forecast errors of wind and geopotential, as we use them, are

$$u = \frac{-K}{\sin\phi} \frac{\partial Z}{\partial \phi} \quad \text{and} \quad \frac{K}{\sin\phi \cos\phi} \frac{\partial Z}{\partial \lambda},$$

in terms of longitude, λ, and latitude, ϕ. Accordingly, except for a common σ_z^2 factor, the geostrophically implied covariances and variances involving the wind f.e.s are

$$\ell(u_i,z_j) = -\frac{\kappa}{\sin\phi_i}\frac{dR}{d\tau}\frac{\partial\tau}{\partial\phi_i} \qquad \ell(v_i,z_j) = \frac{\kappa}{\sin\phi_i\cos\phi_i}\frac{dR}{d\tau}\frac{\partial\tau}{\partial\lambda_i}$$

$$\ell(u_i,v_j) = -\frac{\kappa^2}{\sin\phi_i\sin\phi_j\cos\phi_j}\left(\frac{d^2R}{d\tau^2}\frac{\partial\tau}{\partial\phi_i}\frac{\partial\tau}{\partial\lambda_j} + \frac{dR}{d\tau}\frac{\partial^2\tau}{\partial\phi_i\partial\lambda_j}\right)$$

$$\ell(u_i,u_j) = \frac{\kappa^2}{\sin\phi_i\sin\phi_j}\left(\frac{d^2R}{d\tau^2}\frac{\partial\tau}{\partial\phi_i}\frac{\partial\tau}{\partial\phi_j} + \frac{dR}{d\tau}\frac{\partial^2\tau}{\partial\phi_i\partial\phi_j}\right)$$

$$\ell(v_i,v_j) = \frac{\kappa^2}{\sin\phi_i\cos\phi_i\sin\phi_j\cos\phi_j}\left(\frac{dR}{d\tau^2}\frac{\partial\tau}{\partial\lambda_i}\frac{\partial\tau}{\partial\lambda_j} + \frac{dR}{d\tau}\frac{\partial^2\tau}{\partial\lambda_i\partial\lambda_j}\right)$$

with

$$v(u_i) = \lim_{\tau\to 0}\ell(u_i,u_j) \qquad v(v_i) = \lim_{\tau\to 0}\ell(v_i,v_j).$$

Conditions required for uniqueness of the geostrophically implied, wind f.e. variances (See Thiebaux and Pedder, 1987, p.156.) are

$$\lim_{\tau\to 0}\left(\frac{1}{\tau}\frac{dR}{d\tau} - \frac{d^2R}{d\tau^2}\right) = 0$$

and

$$\lim_{\tau\to 0}\left(\frac{1}{\tau}\frac{dR}{d\tau}\right) = L \quad \text{(finite)}.$$

Since these are properties of all of our candidate correlation basis functions, then, in deriving the variances of the f.e.s of U and V, the separation-dependent factors may be rewritten as

$$\lim_{\tau \to 0} \left[\left(\frac{1}{\tau} \frac{dR}{d\tau} \right) \left(\frac{\partial \tau}{\partial \phi_1} \frac{\partial \tau}{\partial \phi_2} + \tau \frac{\partial^2 \tau}{\partial \phi_1 \partial \phi_2} \right) \right] \qquad \text{for U}$$

and

$$\lim_{\tau \to 0} \left[\left(\frac{1}{\tau} \frac{dR}{d\tau} \right) \left(\frac{\partial \tau}{\partial \lambda_1} \frac{\partial \tau}{\partial \lambda_2} + \tau \frac{\partial^2 \tau}{\partial \lambda_1 \partial \lambda_2} \right) \right] \qquad \text{for V .}$$

Furthermore, all but one of our candidate basis functions is isotropic; and we write them as functions of great-circle-separation

$$\tau = \cos^{-1} \left(\sin\phi_1 \sin\phi_2 + \cos\phi_1 \cos\phi_2 \cos|\lambda_1 - \lambda_2| \right).$$

For these cases,

$$\lim_{\tau \to 0} \left(\frac{\partial \tau}{\partial \theta_1} \frac{\partial \tau}{\partial \theta_2} + \tau \frac{\partial^2 \tau}{\partial \theta_1 \partial \theta_2} \right) = \begin{cases} -\cos^2\phi & \text{for } \theta = \lambda \\ -1 & \text{for } \theta = \phi \end{cases} ;$$

so that

$$\mathcal{C}(u) = \frac{-K^2}{\sin^2\phi} L \qquad \text{and} \qquad \mathcal{C}(v) = \frac{-K^2}{\sin^2\phi} L .$$

Hence, the geostrophically-derived lag-correlation functions for wind-component forecast-errors, may be derived as follows:

$$Q(u_i, z_j) = -\frac{dR}{d\tau} \frac{\partial \tau}{\partial \phi_i} / \sqrt{-L} \qquad Q(v_i, z_j) = \frac{dR}{d\tau} \frac{\partial \tau}{\partial \lambda_i} / \cos\phi_i \sqrt{-L}$$

$$Q(u_i, v_j) = -\left(\frac{d^2R}{d\tau^2} \frac{\partial \tau}{\partial \phi_i} \frac{\partial \tau}{\partial \lambda_j} + \frac{dR}{d\tau} \frac{\partial^2 \tau}{\partial \phi_i \partial \lambda_j} \right) / L \cos\phi_j$$

$$Q(u_i, u_j) = \left(\frac{d^2R}{d\tau^2} \frac{\partial \tau}{\partial \phi_i} \frac{\partial \tau}{\partial \phi_j} + \frac{dR}{d\tau} \frac{\partial^2 \tau}{\partial \phi_i \partial \phi_j} \right) / L$$

$$Q(v_i, v_j) = \left(\frac{d^2R}{d\tau^2} \frac{\partial \tau}{\partial \lambda_i} \frac{\partial \tau}{\partial \lambda_j} + \frac{dR}{d\tau} \frac{\partial^2 \tau}{\partial \lambda_i \partial \lambda_j} \right) / L \cos\phi_i \cos\phi_j$$

and their values computed from the repetitive factors

$$\frac{d^2R}{d\tau^2}\ , \quad \frac{dR}{d\tau}\ , \quad \text{and} \quad L = \lim_{\tau \to 0}\left(\frac{1}{\tau}\frac{dR}{d\tau}\right)$$

and the derivatives of τ with respect to latitude and longitude. The latter are given in Appendix I.

Table 1 presents the isotropic candidate correlation basis functions and the factors required by the above formulations of geostrophic wind correlation functions. Appendix II gives the technical details of the derivations for TOAR.

The reader may confirm that the isotropic, candidate correlation basis functions satisfy the necessary and sufficient conditions for derivation of geostrophic wind correlation functions, by inspection of Table 1, since all basis functions satisfy

$$\lim_{\tau \to 0} \frac{dR}{d\tau} = 0 \qquad \text{and} \qquad \lim_{\tau \to 0} \frac{d^2R}{d\tau^2} \quad \text{is finite.}$$

The former permits application of l'Hôpital's rule to evaluate $\lim_{\tau \to 0}\left(\frac{dR}{d\tau}/\tau\right)$, which then establishes its identity to $\lim_{\tau \to 0}\frac{d^2R}{d\tau^2}$.

For the one anisotropic function considered here, with location separation tensor $\underset{\sim}{\tau} = (\Delta\phi, \Delta\lambda)$, derivation and calculation of geostrophic wind correlation functions are even more straight forward. In this case we assumed that

the geopotential f.e. covariances may be written in terms of the correlation basis function as

$$\mathcal{C}(Z,Z) = \sigma_Z^2 R(\tau) = \sigma_Z^2 \times R_1(\Delta\phi) \times R_2(\Delta\lambda).$$

Consequently, except for a common σ_Z^2 factor, the wind field covariances are

$$\mathcal{C}(V_i, Z_j) = \frac{\kappa}{\sin\phi_i \cos\phi_i} \frac{\partial R_2(\Delta\lambda)}{\partial\lambda_i} \times R_1(\Delta\phi)$$

$$\mathcal{C}(V_i, V_j) = \frac{\kappa^2}{\sin\phi_i \cos\phi_i \sin\phi_j \cos\phi_j} \frac{\partial^2 R_2(\Delta\lambda)}{\partial\lambda_i \partial\lambda_j} \times R_1(\Delta\phi)$$

$$\mathcal{C}(V) = \frac{\kappa^2}{\sin^2\phi \cos^2\phi} \lim_{\Delta\lambda \to 0} \left[\frac{d^2 R_2(\Delta\lambda)}{\partial\lambda_i \partial\lambda_j} \right]$$

etc.

In other words, we have only the signs of the longitude and latitude differences to deal with, rather than the partial derivatives of a scalar measure of location separation. It follows that the lag-correlation functions for the geostrophic wind components are simply

$$Q(V_i, Z_j) = \frac{\partial R_2(\Delta\lambda)}{\partial\lambda_i} R_1(\Delta\phi) / \sqrt{-L_V} \qquad Q(u_i, _j) = -\frac{\partial R_1(\Delta\phi)}{\partial\phi_i} R_2(\Delta\lambda) / \sqrt{-L_u}$$

$$Q(V_i, U_j) = -\frac{\partial R_2(\Delta\lambda)}{\partial\lambda_i} \frac{\partial R_1(\Delta\phi)}{\partial\phi_j} / \sqrt{L_V L_u}$$

$$Q(V_i, V_j) = \frac{\partial^2 R_2(\Delta\lambda)}{\partial\lambda_i \partial\lambda_j} R_1(\Delta\phi) / L_V$$

$$Q(u_i, u_j) = \frac{\partial^2 R_1(\Delta\phi)}{\partial\phi_i \partial\phi_j} R_2(\Delta\lambda) / L_u .$$

Furthermore, following Thiébaux (1976, '77, '81) and Thiébaux, Mitchell and Shantz (1986), we assume the geopotential f.e. correlation basis function has the form

$$\left\{\left[\cos(a_1\Delta\phi) + \frac{c_1}{a_1}\sin(a_1\Delta\phi)\right]\exp(-c_1\Delta\phi)\right\} \times \left\{\left[\cos(a_2\Delta\lambda) + \frac{c_2}{a_2}\sin(a_2\Delta\lambda)\right]\exp(-c_2\Delta\lambda)\right\}$$

with

$$\Delta\phi = |\phi_1 - \phi_2| \quad \text{and} \quad \Delta\lambda = |\lambda_1 - \lambda_2|.$$

Accordingly, the geostrophically implicit wind correlation functions factor; and the factors:

$$\frac{\partial R_1(\Delta\phi)}{\partial\phi_i}, \quad \frac{\partial^2 R_1(\Delta\phi)}{\partial\phi_i\,\partial\phi_j}, \quad L_U \quad \text{and} \quad \frac{\partial R_2(\Delta\lambda)}{\partial\lambda_i}, \quad \frac{\partial^2 R_2(\Delta\lambda)}{\partial\lambda_i\,\partial\lambda_j}, \quad L_V$$

may be obtained from Table 1, lines 2 (or 3), by substituting $\tau = \Delta\phi$ and $\Delta\lambda$.

We note that for both isotropic and anisotropic basis functions, all correlations derived for geostrophic wind components, i.e. both auto- and cross-correlation functions are anisotropic. This is illustrated in Figure 1, where the contours of the SOAR basis function and of the geostrophicly implicit wind f.e. correlation functions are drawn relative to a single analysis point.

3. Reference data sets and function fitting procedures

Observation-minus-forecast differences for radiosonde-derived mandatory level winds and heights were obtained from one year of operational runs of NMC's global spectral model. In their construction, 6-hour forecast values on a 2.5 X 2.5 grid were interpolated bi-linearly to the locations of the radiosonde stations and differenced with the RAOB reports at 00 and 12 GMT. These differences or "forecast errors" (f.e.s) were stored separately for the two synoptic observing times, in four three-month data sets for which we have defined "Winter" as December 1 through February 28(29) and "Summer" as June 1 through August 31.

Northern and Southern Hemisphere data were partitioned by geographic region. In the Northern Hemisphere, longitudinal divisions created four large regions labeled "North America", "Eastern Asia", "Western Asia", and "Europe", which were then partitioned into latitude bands: 0 to 30 N, 25 to 55 N, and 50 to 90 N. Southern Hemisphere data were partitioned by latitude only. Radiosonde coverage strongly influenced the choice of boundary designations shown in Figure 2. Particularly in the Southern Hemisphere, many stations report at only one observing time in each 24 hour period.

For the computation of a regional array of correlations as functions of location separation, station pairs with insufficient common report times were omitted. Of the ninety possible common reports within any season, we required a minimum of fifty in the Northern Hemisphere and 20 in the Southern Hemisphere. In the event that data for a particular day was missing from the covariance summation of the numerator because at least one of the stations of the pair did not have a report on the file, that day was omitted from both variance summations of the denominator, for comparability of variance and covariance statistics.

Our forecast error correlation arrays have had the effects of both the forecast model bias (Thiebaux and Morone, 1989) and the observational error variance (Verzal, Thiebaux, and Morone, 1988) removed in their computation. Removing the model bias allows the correlations to approach zero at large separations. Removing the effect of observational error allows the correlations to go to one at zero separation.

b. fitting correlation function candidates to observed f.e. correlation arrays

A principal issue in our investigation is whether functions which are derived geostrophically from a correlation function for isobaric heights provide optimal representations for isobaric wind/height and wind/wind f.e. correlation structure. Accordingly we developed two sets of

model parameterization algorithms: one to fit candidate geopotential correlation functions (only) to observed geopotential autocorrelation arrays and a second for simultaneous fitting of implicit geostrophic derivatives of suitable basis functions to observed wind/height and wind/wind correlation arrays. Both algorithms compute goodness-of-fit statistics for geopotential, alone, and for wind/height and wind/wind correlations, collectively, on all candidate representations except the FOAR. Thus, with the one exception, our results provide comparable measures of fit, to address the question of the appropriateness of imposing geostrophy on the full, multivariate, correlation matrix. The first-order autoregressive correlation function is parameterized only by the first algorithm, since it does not satisfy requirements for geostrophic correlation derivations.

For the geopotential correlation array fits, the fitting procedure uses the IMSL implementation of a modified Levenberg-Marquardt algorithm for bounded least-squares minimization of the error sum-of-squares. In general, in fitting candidate representations for isobaric lag correlation which are functions of (univariate) distance, the values of the full height/height correlation array are first averaged within adjacent distance intervals, each of length .025 radians. This is a computational expedient; and averaging the data over short intervals of scalar separation is consistent with modeling objectives. Nonetheless, for

comparability of measures of goodness-of-fit with the outcome of simultaneous fittings, root-mean-square differences for the resulting function parameterizations are computed with the original, full correlation arrays.

In the work dealing with the five correlation functions involving wind components:

$R(u,u)$, $R(v,v)$, $R(u,v)$, $R(u,z)$ and $R(v,z)$

candidate basis functions and their derivatives were fitted simultaneously to wind/height and wind/wind f.e. correlation data, using appropriate weights. With autocorrelations and cross-correlations fit simultaneously, cross-correlations are given twice the weight because they represent two terms in the correlation matrix. Again, the fitting procedure uses the IMSL implementation of the bounded least-squares minimization of an error sum-of-squares.

Wind-wind and height-wind correlation function candidates are obtained from candidate basis functions by taking derivatives with respect to the horizontal coordinate axes. Thus they are composed of derivatives of the basis functions with respect to their scalar argument, namely great circle distance (GCD), and partial derivatives of GCD with respect to increments of latitude and longitude. (See Appendix I.)

Wind forecast error correlations exhibit very little structure at large separations. The scale of the patterns evident in f.e. correlation data for the winds is much smaller than that shown by the height data. As an example, Figure 3 shows west-to-east cross-sections of the 500MB U/U forecast error correlation data from Winter 1986-87, for three different Northern Hemisphere regions, plotted as functions of great-circle separation. At separations greater than 0.2 radians, correlation values were small and the arrays were "noisy". Based on this evidence the decision was made to examine and attempt to fit the wind correlations only out to a separation of 0.2 radians.

Although we might have fit the basis functions and their derivatives to the full set of correlation values, our choice was to bin the data to reduce sampling variations due to station distribution and the required computer resources. Since height/wind and wind/wind correlations and their candidate representations are anisotropic, data binning of correlations involving wind f.e.s is based on the vector separation of locations. We averaged radially over intervals of 0.025 radians and over angles in 45 degree increments.

4. Optimal representations of the correlations of wind and geopotential f.e.s

With the expectation that selection of a representation for geopotential f.e. autocorrelation would define the full array of height/height, height/wind, and wind/wind correlation functions, major attention was devoted to determination of parameter values which best fit the candidate basis functions to observed forecast-error correlations of geopotential. Initially we worked with data sets obtained from a tape archive of forecast-minus-RAOB differences for the winter of 1984-85. However, since the major model change implemented in the spring of 1986 had a significant impact of the spatial structure of geopotential f.e. correlations, new data sets were created, starting with December 1, 1986; and the fitting was repeated with this data from the current form of the operational model. Figure 4 contrasts three eras of correlation structures, as well as a slight difference between the structures at 00 and 12 GMT. The two curves illustrate the difference between the negative squared exponential correlation function which has been in the operational suite since 1978, with the parameter value assigned in 1982, and the function found to best fit the 500 mb geopotential correlations computed from the 1984-85 data set. This figure also compares these two correlation model curves with observed correlation values obtained with winter 1986-87 f.e.s. The correlation length scales of the more recent data sets are clearly much greater

than that assumed by the operational analysis which, to the time of this writing, still uses the SQEX function. The contrast between the correlation structures at 00 and 12 GMT is more subtle, although it is evident that the 12 GMT f.e. correlation array drops faster to about 0.20 radians and then flattens out, relative to the 12 GMT array. This difference in correlation structures, between the two principle observing times was apparent in other regions as well, with the most marked contrast in the 0 to 30 latitude band. Figures 5.a and b illustrate regional differences, with 5.a contrasting structures within latitude bands of North America and 5.b illustrating change with longitude for a single latitude band. On the above evidence we maintained separate regional data sets, treated 00 and 12 GMT separately, and worked only with forecast errors from the most recent version of the NMC global model. Finally, Figure 6 demonstrates the dependence of f.e. correlation length scale on isobaric level -- setting the stage for fine tuning parameters of the function used in O.A., in this dimension as well.

A discovery made early in the investigation which ultimately had considerable impact on the modeling of multivariate correlation structure, was that the impression of a non-zero asymptote in geopotential f.e. correlation arrays, which had been ascribed to long wave bias contamination, disappeared when the correlation functions

were plotted out to 0.7 radians. (Compare Figure 4 with Figures 5.a.) Thus we omitted the use of a term to represent a nonzero asymptote, in distinction to the work of Thiébaux, Mitchell and Shantz (1986), and fit the candidates for modeling geopotential correlation out to a great-circle separation of 0.7 radians.

Category I - III models of isobaric spatial correlation structure, described in Section 2, were fit to the interval averaged geopotential correlation values of five of the mandatory pressure levels, for all of the regions designated in the previous section. Root-mean-square differences between each optimally parameterized model and the corresponding observed autocorrelation array were computed as the basis for ranking "model performance" within each region. Figure 7 makes pressure-level/latitude comparisons of the full set of candidate functions, for 850, 500, 250, 100 mb., for the three latitude bands of North America. For geopotential f.e. correlation arrays considered in isolation the function corresponding to a first-order auto-regressive process ranks first among all candidates, in southern and mid-latitudes at all four pressure levels. In the northern latitude band, there is no one function which provides the smallest RMSDs with the observed correlations at all levels.

We note that the fitting done with the autoregressive correlation functions, reported by this figure, used distinct algorithms for the FOAR, SOAR, and TOAR correlation representations each with a single initial parameter array

specified as the starting point for the search in the corresponding parameter space. As we will show, further along in the paper, the three functions can be subsumed by a generalized TOAR representation and the fitting done with a single algorithm. Thus, in viewing Figure 7, FOAR, SOAR, and TOAR results should be regarded together as representing the correlation structure of low-order autoregressive processes, where the TOAR is third-order in the strict sense.

Using the parameters obtained in fitting five of the multivariate correlation basis functions to the 500 mb, mid-latitude region of North America, the implicit height/wind and wind/wind correlation function models were fitted to their corresponding observed correlation arrays, for the same region. The results are illustrated by Figure 8.a. We note that, with the restriction on parameter values imposed by matching wind to height correlations, the present operational correlation function model is outstandingly surpassed in performance by all four other possibilities. With a slight exception, the top performance in this region is scored by the SOAR. These comparisons were repeated with function parameters obtained from simultaneous fitting of derived correlation models to observed height/wind and wind/wind correlation values (omitting the height/height correlation array), with results shown in Figure 8.b. Here the contrasts among basis functions are not as great, indicating that significant improvements may be achieved simply by letting the observed (wind) f.e. correlation

structures influence parameterizations. Nonetheless, the SOAR tied with the TOAR in providing the RMSD best representation for height/wind and wind/wind f.e. correlation structure. Finally we note that a and b of Figure 8 are not comparable with one another because the parameter fits and the goodness-of-fit statistics have been computed for different ranges of location separations. The Z/Z fits that selected the parameters for 8.a used correlations for observed f.e.s at separations as great as .7 radians and computation of goodness-of-fit statistics for the corresponding wind correlations took location separations out to .4 radians. This is in distinction to the simultaneous fits that selected the parameters of 8.b. The latter involved correlation values and computed statistics only for location separations to .2 radians.

As a consequence of the results just reported and a study of the mathematical relationships between several of the candidate functions (See Appendix III.), a major revision of the fitting algorithm was made. The new approach takes advantage of the ubiquitousness of the TOAR, in the sense that the FOAR and SOAR are limiting cases of it. Thus, by searching the parameter space in several regions designated by the algorithm, virtually all options are investigated in a single fitting maneuver; and the unsuitability of the FOAR for geostrophic derivation of wind f.e. correlation representations is no longer a concern, because the parameters are bounded away from the limit at

which the derivatives are not unique. Accordingly we have a single functional form which incorporates the three auto-regressive candidates, in addition to the Kagan function. Comparison of the outcomes that result from fitting the SQEX, FOAR, and the third order polynomial, in terms of root-mean-square differences with interval(bin)-averaged correlations, is provided by Tables 2 and 3. These show RMSD values for five pressure levels, for North America and the Southern Hemisphere, for Northern Hemisphere summer and winter, respectively. At 1000 mb the third order polynomial is slightly better for geopotential. At all levels above 1000 mb, the TOAR is optimal in the parameter region near the FOAR limit, where it provides almost as good a fit as the FOAR itself. The right-hand- sides of these tables give corresponding results of simultaneous fits to height/wind and wind/wind f.e. correlation arrays. Here, without exception, the basis function whose derivative functions provide the best fits to observed correlation arrays is the TOAR with parameters in the "near FOAR" region, in both hemispheres and at all five pressure levels. On the basis of these results we limited ourselves, in subsequent work, to correlation function fitting with the algorithm for the general, third order autoregressive formulation, which searches in those regions of parameter space corresponding to our prime candidate functions.

Tables 4 and 5 present comparative parameter values and RMSDs for 500 mb at mid-latitudes, for North America,

Europe, West Asia, East Asia, and the Southern Hemisphere, for summer and winter, respectively. The comparability among parameter values for a particular function, across regions, is within each row. The comparability of RMSDs, among the candidate functions for a given region, is within each column. Although the values of the constant parameter(s) for each function clearly vary by region, without exception the optimal form for the correlation representation is a TOAR, again with its parameters chosen from the region of the parameter space nearest the FOAR limit. The regional influence on parameter values, evident in these tables is attributed to a combination of factors, one of which is the position of the sun relative to analysis time -- a dependence that can be accounted for operationally by writing parameter values as functions of longitude.

In both summer and winter the parameters selected by the geopotential basis function fits, for North America and the Southern Hemisphere, are remarkably similar. Furthermore, in both seasons, the values of the "c" parameter for the best fitting TOAR suggest that its Northern Hemisphere variation may be represented with a simple harmonic in longitude. The picture presented by the parameter values of the wind correlation function fits is more complicated. Both the "a" and "c" parameter values vary significantly with region; and here there is strong contrast between North American and South Hemisphere values of the "c" parameter.

Section 5. Overview and implications for analysis algorithm updating.

The work reported here has focused on the selection of representations for isobaric correlation structures of observation-minus-forecast differences (f.e.s) of wind and geopotential fields. The principal objective was updating the representations used in the NMC global data assimilation system, for which the 6-hour forecast of the global spectral model provides the "guess fields" for wind and geopotential analyses. Geostrophic coupling of f.e.s is imposed in the derivation of the wind-wind and wind-height correlation functions, from a basic Z-Z forecast-error correlation function. To date, the derived correlation representations have been used operationally with a single set of parameter values -- identical for height and wind f.e. correlations. One of our purposes was to determine whether this is in reasonable agreement with observed f.e. correlation structure. In fact, the contrast in parameter values selected as best-fitting the f.e. correlation arrays of geopotential, on the one hand, and the winds, on the other, points up the fact that the increments between observations and forecast values are not fully geostrophic in their ensemble properties. (Compare the a and b sections of Tables 4 and 5.) In Figure 9 we demonstrate the contrast between the U/U correlation length scale implicit in the simultaneous wind parameterization of the best fitting TOAR and that obtained by fitting the basis function to the geopotential f.e. correlation array. It goes without saying

that the scales are significantly different and that the use of one parameter set in the role of the other would be seriously misrepresenting the ensemble structure of the observation-minus-forecast increment field.

The foregoing results clearly suggest the use of a single functional form, with distinct parameter sets for heights and winds. This recommendation of an algorithm for multivariate optimum interpolation of wind and geopotential f.e.s to the model grid, to produce analysed fields for reinitialization will require testing, to assure its compatability with other components of the data assimilation system. For practical purposes, the performance of the third-order autoregressive correlation function, with parameters selected by fitting to geopotential f.e. correlation arrays is indistinguishable from the fits of the first-order function. And there is no doubt that the suite of five wind/wind and wind/height correlation functions derived from the TOAR, with parameters in the "near FOAR" region, provides the best fits to corresponding arrays of observed correlation values. Thus the TOAR is the function of choice.

The most prominent feature of the functional form which clearly provides the optimal basis for representations of the correlation structures of these hichly complex forecast-error fields, is its simplicity. Despite the anticipated advantages of an anisotropic function for geopotential and

of several adjustable parameters in closely related correlation structure models, correlation arrays calculated from the Center's operational forecast-minus-observation differences have self-selected a relatively simple two parameter model. This result, together with the evidence that the most recent major change in NMC's global spectral model led to a significant change in the ensemble spatial structure of its forecast-errors, might have been anticipated as a consequence of improvements in forecast accuracy: The closer numerical weather prediction comes to the true evolution of atmospheric states, the closer the discrepancies of NWP forecasts and observations come to pure (microscale + observation error) noise processes. The higher order components of NWP models and of the most dominant atmospheric scales are increasingly cleanly differenced. Thus the spatial scales of the f.e. decrease (toward zero) and smaller fractions of the analysis increments are relevant to correcting forecast values at any given distance from their observation. The simple negative exponential, from a one parameter, first order process, namely the FOAR, is characteristic of the improvement in short range forecasting of geopotential fields. The use of a function closely mimicing this behavior will constitute an update of our data assimilation process compatable with present forecast skill.

The fact that wind/height and wind/wind correlations are not as well represented by functions that are direct

geostrophic derivatives of the function which provides the best representation for height/height correlations does not, by itself, jeopardize the positive definiteness of the full covariance matrix. What it says is that the ensemble relationships between the forecast-minus-observation increments for geopotential and the wind components is not completely geostrophic; and thus it may not be appropriate to impose full geostrophic balance on the functions selected to represent those relationships. Consider that if it were possible to use exactly the covariance structure of the discrepancy between six-hour forecast fields and reports from the global observing system, that would be the optimal choice for global objective analysis. Since that is not possible, we model the covariance structure -- as closely as possible to the way it shows up in observed f.e. covariance arrays. With evidence that the height and wind f.e.s are not in complete geostrophic balance, it is appropriate to use covariance structure which does not impose full geostrophy. In particular, we choose the functions which provide the best fit to the data.

Our experience with change in forecast error correlation structure, brought by change in the global forecast cycle over a twelve month period, and the evidence for change in correlation scales with time of year, confirm the requirement for automation of correlation model updating. We have identified a common framework for accessing the full range of our candidate functions in a single fitting

algorithm, making use of the fact that all (lower order) autoregressive correlation functions are special cases of a TOAR correlation function. Accordingly, reparameterizations can be carried out in a highly efficient manner, with the full generality of our suite of representations. Keeping the analysis system in step with evolving characteristics of NMC's global forecast system, can thus be made a relatively straightforward housekeeping operation.

Appendix I

For

$$\tau = \cos^{-1}\left(\sin\phi_i \sin\phi_j + \cos\phi_i \cos\phi_j \cos|\lambda_i - \lambda_j|\right)$$

we derive the components

$$\frac{\partial \tau}{\partial \theta_i}, \quad \frac{\partial \tau}{\partial \theta_j}, \quad \text{and} \quad \frac{\partial^2 \tau}{\partial \theta_i \partial \theta_j}, \quad \text{for} \quad \theta = \lambda, \phi,$$

and demonstrate that

$$\lim_{\tau \to 0}\left(\frac{\partial \tau}{\partial \theta_i}\frac{\partial \tau}{\partial \theta_j} + \tau \frac{\partial^2 \tau}{\partial \theta_i \partial \theta_j}\right) = \begin{cases} -\cos^2\phi, & \text{for } \theta = \lambda \\ -1, & \text{for } \theta = \phi \end{cases}.$$

Let $\tau = \cos^{-1} q$ define

$$q = \sin\phi_i \sin\phi_j + \cos\phi_i \cos\phi_j \cos|\Delta\lambda|$$

for which

$$\frac{\partial q}{\partial \lambda_i} = -\cos\phi_i \cos\phi_j \sin|\Delta\lambda| \operatorname{sign}(\lambda_i - \lambda_j) = -\frac{\partial q}{\partial \lambda_j}$$

$$\frac{\partial^2 q}{\partial \lambda_i \partial \lambda_j} = \cos\phi_i \cos\phi_j \cos|\Delta\lambda|$$

and

$$\frac{\partial q}{\partial \phi_i} = \cos\phi_i \sin\phi_j - \sin\phi_i \cos\phi_j \cos|\Delta\lambda|$$

$$\frac{\partial q}{\partial \phi_j} = \sin\phi_i \cos\phi_j - \cos\phi_i \sin\phi_j \cos|\Delta\lambda|$$

$$\frac{\partial^2 q}{\partial \phi_i \partial \phi_j} = \cos\phi_i \cos\phi_j + \sin\phi_i \sin\phi_j \cos|\Delta\lambda|.$$

Now, since $\cos\tau = q$ then, for $\theta = \lambda$ or ϕ,

$$\frac{\partial \tau}{\partial \theta} = -\frac{1}{\sin\tau}\frac{\partial q}{\partial \theta}$$

$$\frac{\partial^2 \tau}{\partial \theta_i \partial \theta_j} = -\frac{\cos\tau}{\sin^3\tau}\left(\frac{\partial q}{\partial \theta_i}\right)\left(\frac{\partial q}{\partial \theta_j}\right) - \frac{1}{\sin\tau}\left(\frac{\partial^2 q}{\partial \theta_i \partial \theta_j}\right)$$

and

$$\frac{\partial \sigma}{\partial \theta_i}\frac{\partial \sigma}{\partial \theta_j} + \sigma\frac{\partial^2 \sigma}{\partial \theta_i \partial \theta_j} = \left(\frac{1}{\sin^2\sigma} - \frac{\sigma\cos\sigma}{\sin^3\sigma}\right)\left(\frac{\partial \varphi}{\partial \theta_i}\right)\left(\frac{\partial \varphi}{\partial \theta_j}\right) - \frac{\sigma}{\sin\sigma}\left(\frac{\partial^2 \varphi}{\partial \theta_i \partial \theta_j}\right);$$

and we can put this together with the foregoing to obtain

$$\text{(AI.1)}\quad \frac{\partial \sigma}{\partial \lambda_i}\frac{\partial \sigma}{\partial \lambda_j} + \sigma\frac{\partial^2 \sigma}{\partial \lambda_i \partial \lambda_j} = \left(\frac{\sin\sigma - \sigma\cos\sigma}{\sin^3\sigma}\right)\cos^2\phi_i \cos^2\phi_j \sin^2|\Delta\lambda| - \frac{\sigma}{\sin\sigma}\cos\phi_i \cos\phi_j \cos|\Delta\lambda|$$

and

$$\text{(AI.2)}\quad \frac{\partial \sigma}{\partial \phi_i}\frac{\partial \sigma}{\partial \phi_j} + \sigma\frac{\partial^2 \sigma}{\partial \phi_i \partial \phi_j} = \left(\frac{\sin\sigma - \sigma\cos\sigma}{\sin^3\sigma}\right)\left(\cos\phi_i\sin\phi_j - \sin\phi_i\cos\phi_j\cos|\Delta\lambda|\right)\times \left(\sin\phi_i\cos\phi_j - \cos\phi_i\sin\phi_j\cos|\Delta\lambda|\right) - \frac{\sigma}{\sin\sigma}\left(\cos\phi_i\cos\phi_j + \sin\phi_i\sin\phi_j\cos|\Delta\lambda|\right)$$

To determine the limits of thses two quantities as $\sigma \to 0$, i.e. as (λ_i, ϕ_i) and (λ_j, ϕ_j) approach a common value, (λ, ϕ) say, we will require the following two limiting values:

$$\lim_{\sigma\to 0}\left(\frac{\sigma}{\sin\sigma}\right) = \lim_{\sigma\to 0}\left(\frac{1}{\cos\sigma}\right) = 1$$

and

$$\lim_{\sigma\to 0}\left(\frac{\sin\sigma - \sigma\cos\sigma}{\sin^3\sigma}\right) = \lim_{\sigma\to 0}\left(\frac{\cos\sigma - \cos\sigma + \sigma\sin\sigma}{3\sin^2\sigma\cos\sigma}\right)$$

$$= \lim_{\sigma\to 0}\left(\frac{\sigma}{3\sin\sigma\cos\sigma}\right) = \lim_{\sigma\to 0}\left(\frac{1}{3\cos^2\sigma - 3\sin^2\sigma}\right) = \frac{1}{3},$$

obtained by repeated applications of l'Hôpital's rule.

Since both of the above are finite, the limiting values of (AI.1) and (AI.2) are determined by

$$\lim_{\sigma\to 0}\left(\cos^2\phi_i \cos^2\phi_j \sin^2|\Delta\lambda|\right) = 0$$

$$\lim_{\sigma\to 0}\left(\cos\phi_i \cos\phi_j \cos|\Delta\lambda|\right) = \cos^2\phi$$

$$\lim_{v \to 0} [(\cos\phi_i \sin\phi_j - \sin\phi_i \cos\phi_j \cos|\Delta\lambda|) \times (\sin\phi_i \cos\phi_j - \cos\phi_i \sin\phi_j \cos|\Delta\lambda|)] = 0$$

and

$$\lim_{v \to 0} (\cos\phi_i \cos\phi_j + \sin\phi_i \sin\phi_j \cos|\Delta\lambda|) = 1 .$$

Consequently,

$$\lim_{v \to 0} \left(\frac{\partial v}{\partial \lambda_i} \frac{\partial v}{\partial \lambda_j} + v \frac{\partial^2 v}{\partial \lambda_i \partial \lambda_j} \right) = - \cos^2\phi$$

and

$$\lim_{v \to 0} \left(\frac{\partial v}{\partial \phi_i} \frac{\partial v}{\partial \phi_j} + v \frac{\partial^2 v}{\partial \phi_i \partial \phi_j} \right) = -1 .$$

Appendix II

For

$$R(\tau) = [\alpha e^{-a\tau}\cos(b\tau) + \beta e^{-a\tau}\sin(b\tau) + \gamma e^{-c\tau}]/(\alpha+\gamma)$$

with the three parameter vector function $(\alpha,\beta,\gamma) = g(a,b,c)$ given by

$$\alpha = (3a^2 - b^2 - c^2)bc$$
$$\beta = (a^2 - 3b^2 - c^2)ac$$
$$\gamma = -2(a^2+b^2)ab$$

we establish that

$$\text{(AII.1)}\quad \frac{dR}{d\tau} = -(a^2+b^2)c[(a^2-b^2-c^2)e^{-a\tau}\sin(b\tau) - 2ab\,e^{-a\tau}\cos(b\tau) + 2ab\,e^{-c\tau}]/(\alpha+\gamma)$$

and

$$\text{(AII.2)}\quad \frac{d^2R}{d\tau^2} = (a^2+b^2)c[(a^2+b^2-c^2)a\,e^{-a\tau}\sin(b\tau) + (a^2+b^2+c^2)b\,e^{-a\tau}\cos(b\tau) - 2abc\,e^{-c\tau}]/(\alpha+\gamma).$$

Clearly,

$$\frac{dR}{d\tau} = [-(\alpha b+\beta a)e^{-a\tau}\sin(b\tau) + (-\alpha a+\beta b)e^{-a\tau}\cos(b\tau) - \gamma c e^{-c\tau}]/(\alpha+\gamma)$$

and

$$\frac{d^2R}{d\tau^2} = \{[(\alpha b+\beta a)a + (\alpha a-\beta b)b]e^{-a\tau}\sin(b\tau) - [(\alpha b+\beta a)b + (-\alpha a+\beta b)a]e^{-a\tau}\cos(b\tau) + \gamma c^2 e^{-c\tau}\}/(\alpha+\gamma)$$

Substituting α,β,γ in the coefficients of

$$e^{-a\tau}\sin(b\tau),\quad e^{-a\tau}\cos(b\tau),\quad e^{-c\tau}$$

we obtain, first

$$(\alpha b+\beta a) = [(3a^2-b^2-c^2)b^2 + (a^2-3b^2-c^2)a^2]c$$
$$= [a^4 - (b^2+a^2)c^2 + b^4]c$$
$$= (a^2+b^2)(a^2-b^2-c^2)c$$

$$(\alpha a - \beta b) = [(3a^2 - b^2 - c^2) - (a^2 - 3b^2 - c^2)]\, abc$$
$$= 2(a^2 + b^2)\, abc$$
$$\gamma_c = -2(a^2 + b^2)\, abc$$

which establishes (AII.1), and second

$$[(\alpha b + \beta a)a + (\alpha a - \beta b)b] = 2\alpha ab + \beta(a^2 - b^2)$$
$$= 2(3a^2 - b^2 - c^2)ab^2 c + (a^2 - 3b^2 - c^2)(a^2 - b^2)\, ac$$
$$= (2a^2 b^2 + b^4 - b^2 c^2 + a^4 - a^2 c^2)\, ac$$
$$= [(a^2 + b^2)^2 - (a^2 + b^2)c^2]\, ac$$

$$[(\alpha b + \beta a)b + (-\alpha a + \beta b)a] = \alpha(b^2 - a^2) + 2\beta ab$$
$$= (3a^2 - b^2 - c^2)(b^2 - a^2)\, bc + 2(a^2 - 3b^2 - c^2)a^2 bc$$
$$= -(2a^2 b^2 + a^4 + b^4 + b^2 c^2 + a^2 c^2)\, bc$$
$$= -[(a^2 + b^2)^2 + (a^2 + b^2)c^2]\, bc$$
$$= -(a^2 + b^2)(a^2 + b^2 + c^2)\, bc$$

and

$$\gamma_{c^2} = -2(a^2 + b^2)\, abc^2$$

which establishes (AII.2).

Appendix III

This appendix shows how the TOAR function can be used to represent the SOAR, FOAR, and Kagan functions and how, over a restricted parameter range, a relatively exhaustive search may be made for a "global" minimum fit. As a consequence it is possible for a single function and fitting code to locate minima previously found by comparing fits of several functions.

The TOAR function for height-height correlations is

(AIII.1) $$R(\tau)=\frac{\{\alpha\cos(b\tau)+\beta\sin(b\tau)\}\exp(-a\tau)+\gamma\exp(-c\tau)}{\alpha+\gamma}$$

where

$$\alpha=bc\left(3a^2-b^2-c^2\right)$$
$$\beta=ac\left(a^2-3b^2-c^2\right)$$
$$\gamma=-2ab\left(a^2+b^2\right)$$

The SOAR function for height-height correlations is

(AIII.2) $$R(\tau)=\{\cos(a\tau)+(c/a)\sin(a\tau)\}\exp(-c\tau)$$

which may be obtained as the limit of TOAR as c approaches infinity by applying L'Hôpital's rule, dropping the second exponential term which now has a zero coefficient, and relabeling the remaining constants.

The FOAR function for height-height correlations is

(AIII.3) $$R(\tau)=\exp(-a\tau)$$

which may be obtained as the limit of TOAR as a approaches infinity by applying L'Hôpital's rule, dropping the first exponential term which is everywhere zero, and relabeling the remaining constant.

Kagan's function, which was suggested for height-height cor-

relations by Gandin (1988), is

(AIII.4)
$$R(\tau)=\left(1+a\tau+\frac{(a\tau)^2}{3}\right)\exp(-a\tau)$$

which may be obtained as a special case of TOAR by setting $b=0$ and $c=a$ and applying l'Hôpital's rule three times.

The TOAR function (and the Kagan function as a special case of TOAR) have the property that the third derivative of the function with respect to the radius is continuous as one passes through $\tau=0$. This implies that derivative properties of the wind (divergence and vorticity) are modified smoothly by an analysis based on these functions. The third derivative of SOAR is discontinuous, but the second derivative is continuous at $\tau=0$; the second derivative of the FOAR is discontinuous. As a result of these derivative properties one should remember that, although a TOAR subprogram can be made to calculate the SOAR and FOAR functions as special cases, the derivative properties of TOAR when all parameters are finite do not hold in these limits.

Our experience indicates that in most cases the f. e. correlation data are best fit by TOAR with $b=0$ or SOAR with $a=0$, and that, in cases with a reasonable amount of data, fits with these restrictions are almost as good as the best unrestricted fits we have obtained. We also find that the TOAR with $b=0$ frequently has two local minima, and with $b\neq0$ there is often at least one more minimum, usually not as good as the others. While it is difficult to prescribe a general search for a global minimum with the unrestricted functions, under these restrictions the SOAR search becomes one-dimensional and relatively straightforward and

the TOAR search becomes a relatively well-behaved two-dimensional search. Thus we concentrate primarily on these restricted cases of SOAR and TOAR. The TOAR function with $b=0$ is, by application of l'Hôpital's rule to (AIII.1) above,

(AIII.5) $$R(\tau)=\frac{(\alpha+\beta\alpha\tau)\exp(-\alpha\tau)+\gamma\exp(-c\tau)}{\alpha+\gamma}$$

where

$$\alpha=c\left(3a^2-c^2\right)$$
$$\beta=ac\left(a^2-c^2\right)$$
$$\gamma=-2a^3$$

The SOAR function with $a=0$ is, by application of l'Hôpital's rule to (AIII.2) above,

(AIII.6) $$R(\tau)=(1+c\tau)\exp(-c\tau)$$

As above, the TOAR approaches the limiting cases of SOAR or FOAR functions when one of the parameters approaches infinity. In order to allow the SOAR limit to be reached and to cast the search problem in a more tractable form, it is convenient to express TOAR in terms of the ratio of a to c:

(AIII.7) $$R(\tau)=\frac{\left\{\left(3r^2-1\right)+\left(r^2-1\right)a\tau\right\}\exp(-a\tau)-2r^3\exp(-a\tau/r)}{3r^2-1-2r^3}$$

where

$$r=\frac{a}{c}$$

We have chosen this form because in simultaneous wind-height fitting we might want to include the SOAR limit $r\to 0$ in the search but we would not be interested in reaching the FOAR limit $r\to\infty$. If the FOAR limit is to be included, an additional substitution

of variables would be necessary. Since the denominator of (AI-II.7) becomes zero when $r=1$ (Kagan's function), we use the simpler form (AIII.4) above. The TOAR with $b=0$ is in a sense smoothest near $r=0$ when $r=1$ and less smooth as we approach the SOAR limit $r\to 0$ or the FOAR limit $r\to\infty$.

The search procedure for the restricted TOAR must allow us to find all the local minima. For a given value of r we normally find a single minimum as we vary a. Because the fitting process is nonlinear, with unusual data distributions there could be any number of minima, but for reasonable amounts of data there is only one. Turning now to the search for minima in r of the minimum with respect to a, we might expect two minima based on the quadratic coefficients in the numerators of the coefficients, less one because all the coefficients are monotonic in the range of interest $r\geq 0$, and we might expect that, because the denominator has its only two roots in this range at $r=1$, there might be one or two additional numerator roots. By this argument we expect possibly three minima. This analysis is not rigorous because r also appears inside the exponential, and because the fitting process is nonlinear, we must again assume a reasonable distribution of data. To cover the realistic possibilities we could search in 3 ranges on either side of the Kagan case; in practise we have made the intervals near the Kagan case narrow and combined them: since the variation of the function and the fit through this range is slow, if there were 2 minima in this range they couldn't differ significantly. Our intervals are

1. at or near the SOAR limit $(0\leq r\leq 0.1)$

2. between SOAR and Kagan ($0.1 \leq r \leq 0.625$)

3. near Kagan ($0.625 \leq r \leq 1.6$)

4. between Kagan and FOAR ($1.6 \leq r \leq 10.0$)

5. near the FOAR limit ($10.0 \leq r \leq 100.0$)

If we wish to avoid the discontinuous third derivative of SOAR at $\tau=0$, we set the lower limit of interval 1 to a small positive value such as 0.01. In fitting this function to data we find that in most cases there are 2 local minima, one at or near the SOAR limit (intervals 1 or 2) and one near the FOAR limit (intervals 5 or 6). In a few cases there is one minimum fit at or near Kagan's function (interval 3). Thus, to find the global minimum we must search separately in at least two ranges of the parameter ratio to compare the two local minima that normally exist. Our choice of intervals is intended to having any one interval contain both a relative minimum and a relative maximum which could result in a false minimum from the fitting procedure.

References

Bell, R. S. and A. Dickinson (1987): The Meteorological Office operational numerical weather prediction system. Scientific Paper, U.K. Meteorological Office, No. 41.

Bergman, K. H. (1979): Multivariate analysis of temperatures and winds using optimum interpolation. Mon. Weather Rev., 107, 1423-1444.

Bourke, W. et al (1989): Mon. Weather Rev., 117, in press.

Dey, C. H. and L. L. Morone (1985): Evolution of the National Meteorological Center global data assimilation system. Mon. Weather Rev., 113, 304-318.

Goerss, J. (1989): Personal communication

Hollingsworth, A. and P. Lönnberg (1986): The statistical structure of short-range forecast errors as determined from radiosonde data. Part I: The wind field. Tellus, 38A, 111-136.

Lönnberg, P. and A. Hollingsworth (1986): The statistical structure of short-range forecast errors as determined from radiosonde data. Part II: The covariance of height and wind errors. Tellus, 38A, 137-161.

Rutherford, I. D. (1972): Data assimilation by statistical interpolation of forecast error fields. J. Atmos. Sci., 29, 809-815.

Schlatter, T. W. (1975): Some experiments with a multivariate statistical objective analysis scheme. Mon. Weather Rev., 103, 246-257.

Thiébaux, H. J., H. L. Mitchell and D. W. Shantz (1986): Horizontal structure of hemispheic forecast error correlations for geopotential and temperature. Mon. Weather Rev., 114, 1048-1066.

Table 1. Properties of isotropic candidate correlation basis functions, for positive location separation, $\tau > 0$.

Basis function $R(\tau)$	$dR(\tau)/d\tau$	$d^2R(\tau)/d\tau^2$	$-L$
Squared exponential (SQEX) $\exp(-b\tau^2)$	$-2b\tau \exp(-b\tau^2)$	$2b(2b\tau^2-1)\exp(-b\tau^2)$	$2b$
Second order autoregressive (SOAR) $[\cos(a\tau) + \frac{c}{a}\sin(a\tau)]\exp(-c\tau)$	$-\left(\frac{a^2+c^2}{a}\right)\sin(a\tau)\exp(-c\tau)$	$-(a^2+c^2)[\cos(a\tau) - \frac{c}{a}\sin(a\tau)]\exp(-c\tau)$	(a^2+c^2)
and for $a = 0$: $(1+c\tau)\exp(-c\tau)$	$-c^2\tau \exp(-c\tau)$	$-c^2(1-c\tau)\exp(-c\tau)$	c^2
Third order autoregressive (TOAR) $\gamma\exp(-c\tau) + [\alpha\cos(b\tau) + \beta\sin(b\tau)]\exp(-a\tau)$ where $(\alpha,\beta,\gamma) = g(a,b,c)$	$(a^2+b^2)\frac{c}{d}\{2ab\exp(-c\tau) - \exp(-a\tau)x$ $[(a^2-b^2-c^2)\sin(b\tau) + 2ab\cos(b\tau)]\}$	$(a^2+b^2)\frac{c}{d}\{-2abc\exp(-c\tau) + \exp(-a\tau)x$ $[a(a^2+b^2-c^2)\sin(b\tau) + b(a^2+b^2+c^2)\cos(b\tau)]\}$	$(a^2+b^2)b\frac{c}{d}x$ $(a^2+b^2+c^2-2ac)$
Inverse polynomial of order 3 in τ^2, P_3 : $[1+a\tau^2+b\tau^4+c\tau^6]^{-1}$	$\frac{2a\tau + 4b\tau^3 + 6c\tau^5}{[1+a\tau^2+b\tau^4+c\tau^6]^2}$	$\frac{d^2P_3}{a\tau^2}P_3^{-2} - 2\left(\frac{dP_3}{d\tau}\right)^2 P_3^{-3}$	$2a$
Inverse polynomial of order 5 in τ^2, P_5 : $[1+a\tau^2+b\tau^4+c\tau^6+d\tau^8+e\tau^{10}]^{-1}$	$\frac{2a\tau + 4b\tau^3 + 6c\tau^5 + 8d\tau^7 + 10e\tau^9}{[1+a\tau^2+b\tau^4+c\tau^6+d\tau^8+e\tau^{10}]^{-2}}$	$\frac{d^2P_5}{d\tau^2}P_5^{-2} - 2\left(\frac{dP_5}{d\tau}\right)^2 P_5^{-3}$	$2a$
Kagan's function: $[1+a\tau + (a\tau)^2/3]\exp(-a\tau)$	$-(a^2\tau/3)(1+a\tau)\exp(-a\tau)$	$(a^2/3)[(a\tau)^2 - a\tau - 1]\exp(-a\tau)$	$a^2/3$

Table 2. Root-mean-square differences between candidate functions and interval(bin)-averaged correlations for mid-latitudes at 00GMT for No. Hemisphere summer.

Function/Level	Fits to Z/Z correlation values only		Simultaneous fits to Z/U, Z/V, U/U, V/V, and U/V correlation values	
	North America	So. Hemisphere	North America	So. Hemisphere
SQEX/1000	.0134	.0344	.0290	.0655
850	.0135	.0199	.0215	.0245
500	.0088	.0242	.0150	.0423
250	.0061	.0224	.0169	.0580
100	.0212	.0313	.0487	.0478
FOAR/1000	.0055	.0353		
850	.0024	.0117		
500	.0012	.0191		
250	.0013	.0182		
100	.0060	.0185		
TOAR near FOAR				
1000	.0056	.0350	.0164	.0570
850	.0025	.0117	.0065	.0221
500	.0012	.0191	.0068	.0299
250	.0014	.0182	.0042	.0301
100	.0062	.0186	.0082	.0260
TOAR near SOAR				
1000	.0096	.0346	.0190	.0652
850	.0073	.0146	.0083	.0234
500	.0042	.0208	.0070	.0349
250	.0034	.0197	.0054	.0317
100	.0139	.0244	.0244	.0351
TOAR near Kagan				
1000	.0107	.0344	.0190	.0652
850	.0089	.0160	.0127	.0239
500	.0055	.0217	.0086	.0376
250	.0041	.0204	.0087	.0408
100	.0162	.0263	.0345	.0511
TOAR best of five				
1000	.0056	.0344	.0164	.0570
850	.0025	.0117	.0065	.0221
500	.0012	.0191	.0068	.0299
250	.0014	.0182	.0042	.0301
100	.0062	.0186	.0082	.0260
POLY/1000	.0054	.0337	.0189	.0651
850	----	.0133	----	.0232
500	----	.0197	----	.0359
250	----	.0185	----	.0402
100	----	.0197	----	.0478

Table 3. Root-mean-square differences between candidate functions and interval(bin)-averaged correlations for mid-latitudes at 00GMT for No. Hemisphere winter.

Function/Level	Fits to Z/Z correlation values only		Simultaneous fits to Z/U, Z/V, U/U, V/V, and U/V correlation values	
	North America	So. Hemisphere	North America	So. Hemisphere
SQEX/1000	.0045	.0146	.0411	.0307
850	------	.0092	-----	.0281
500	.0092	.0155	.0137	.0389
250	.0041	.0153	.0243	.0361
100	.0073	.0144	.0294	.0344
FOAR/1000	.0015	.0170		
850	.0005	.0084		
500	.0010	.0081		
250	.0006	.0093		
100	.0006	.0107		
TOAR near FOAR				
1000	.0014	.0162	.0209	.0270
850	.0005	.0077	.0027	.0249
500	.0010	.0081	.0034	.0301
250	.0006	.0094	.0052	.0259
100	.0006	.0107	.0064	.0216
TOAR near SOAR				
1000	.0021	.0150	.0269	.0301
850	.0029	.0072	.0049	.0251
500	.0046	.0107	.0040	.0348
250	.0016	.0114	.0074	.0331
100	.0028	.0118	.0171	.0331
TOAR near Kagan				
1000	.0027	.0148	.0340	.0300
850	.0041	.0075	.0087	.0260
500	.0059	.0119	.0067	.0368
250	.0022	.0123	.0131	.0350
100	.0040	.0124	.0270	.0331
TOAR best of five				
1000	.0014	.0148	.0209	.0270
850	.0005	.0072	.0027	.0249
500	.0010	.0081	.0034	.0301
250	.0006	.0094	.0052	.0259
100	.0006	.0107	.0064	.0216
POLY/1000	.0014	.0147	.0325	.0298
850	----	.0071	----	.0254
500	----	.0089	----	.0353
250	----	.0100	----	.0335
100	----	.0111	----	.0328

Table 4. Parameter values and root-mean-square differences with observed 500 mb correlation values in Northern Hemisphere summer

a. from geopotential basis function fits

Correlation Model	parameter(s)	REGION North America	Europe	West Asia	East Asia	Southern Hemisphere
TOAR (b=0) near FOAR	a	757.	1000.	1000.	1000.	947.
	c	8.	24.	33.	16.	9.
	RMSD	.0012	.0048	.0031	.0025	.0191
TOAR (b=0) near SOAR	a	16.	55.	73.	35.	19.
	c			0.	0.	
	RMSD	.0042	.0073	.0046	.0060	.0208
TOAR (b=0) near Kagan	a	20.	60.	89.	43.	23.
	c	31.	109.	142.	69.	37.
	RMSD	.0055	.0081	.0050	.0072	.0217
Best TOAR (b=0)	a	757.	1000.	1000.	1000.	947.
	c	8.	24.	33.	16.	9.
	RMSD	.0012	.0048	.0031	.0025	.0191

b. from wind correlation function fits

TOAR (b=0) near FOAR	a	68.	81.	101.	81.	73.
	c	5.	10.	1.	2.	1.
	RMSD	.0068	.0090	.0080	.0065	.0299
TOAR (b=0) near SOAR	a	18.	25.	25.	20.	233.
	c		251.	0.	0.	
	RMSD	.0070	.0096	.0096	.0083	.0349
TOAR (b=0) near Kagan	a	28.	37.	38.	32.	39.
	c	45.	58.	61.	51.	63.
	RMSD	.0086	.0103	.0116	.0107	.0376
Best TOAR (b=0)	a	68.	81.	101.	81.	73.
	c	5.	10.	1.	2.	1.
	RMSD	.0068	.0090	.0080	.0065	.0299

Table 5. Parameter values and root-mean-square differences with observed 500 mb correlation values in Northern Hemisphere winter,

a. from geopotential basis function fits

Correlation Model	parameter(s)	REGION North America	Europe	West Asia	East Asia	Southern Hemisphere
TOAR (b=0) near FOAR	a	854.	1000.	1000.	1000.	903.
	c	9.	22.	59.	12.	9.
	RMSD	.0010	.0022	.0090	.0025	.0081
TOAR (b=0) near SOAR	a	18.	49.	180.	28.	18.
	c					
	RMSD	.0042	.0050	.0096	.0063	.0107
TOAR (b=0) near Kagan	a	22.	60.	214.	34.	22.
	c	36.	96.	343.	54.	35.
	RMSD	.0059	.0059	.0096	.0047	.0119
Best TOAR (b=0)	a	854.	1000.	1000.	1000.	903.
	c	9.	22.	59.	12.	9.
	RMSD	.0010	.0022	.0090	.0025	.0081

b. from wind correlation function fits

TOAR (b=0) near FOAR	a	105.	112.	110.	111.	82.
	c	4.	9.	1.	2.	1.
	RMSD	.0034	.0058	.0071	.0043	.0301
TOAR (b=0) near SOAR	a	24.	27.	25.	25.	29.
	c					
	RMSD	.0040	.0056	.0090	.0051	.0348
TOAR (b=0) near Kagan	a	38.	42.	39.	40.	49.
	c	60.	67.	62.	64.	79.
	RMSD	.0067	.0080	.0114	.0078	.0368
Best TOAR (b=0)	a	105.	112.	110.	111.	82.
	c	4.	9.	1.	2.	1.
	RMSD	.0038	.0058	.0071	.0043	.0301

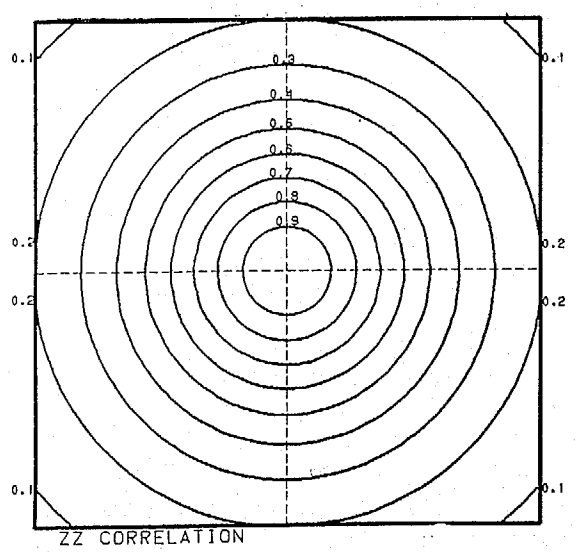
ZZ CORRELATION

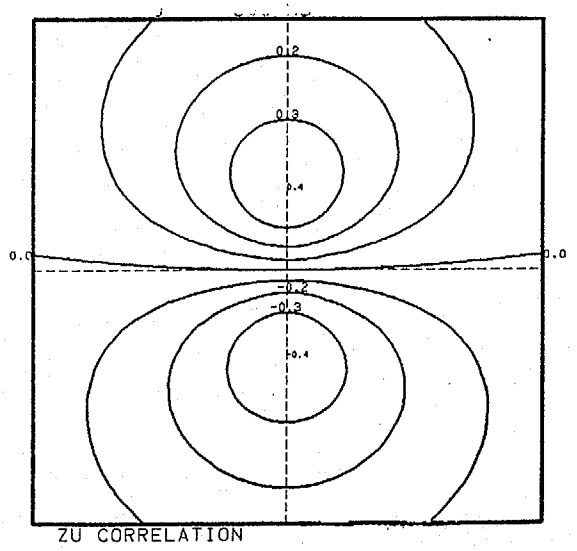
ZU CORRELATION

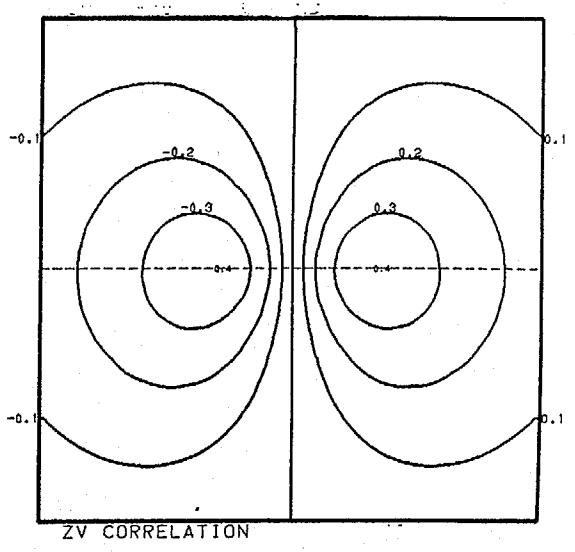
ZV CORRELATION

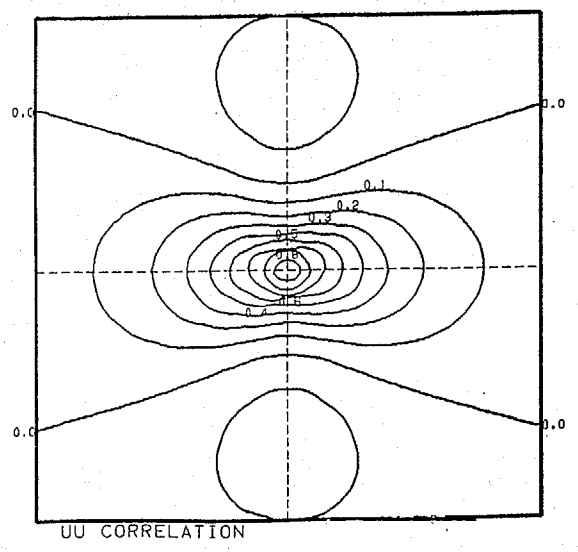
UU CORRELATION

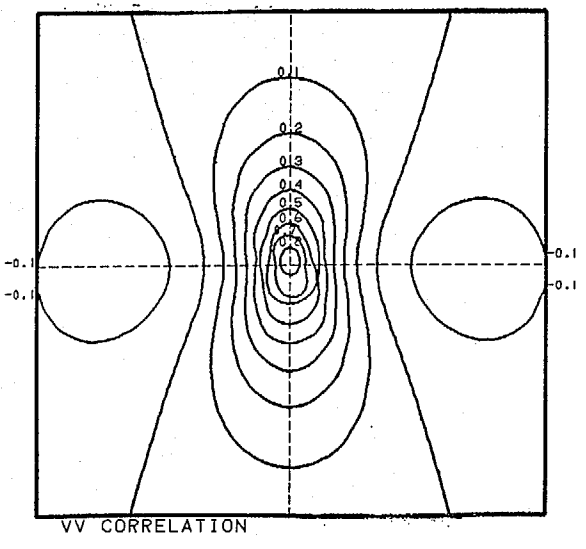
VV CORRELATION

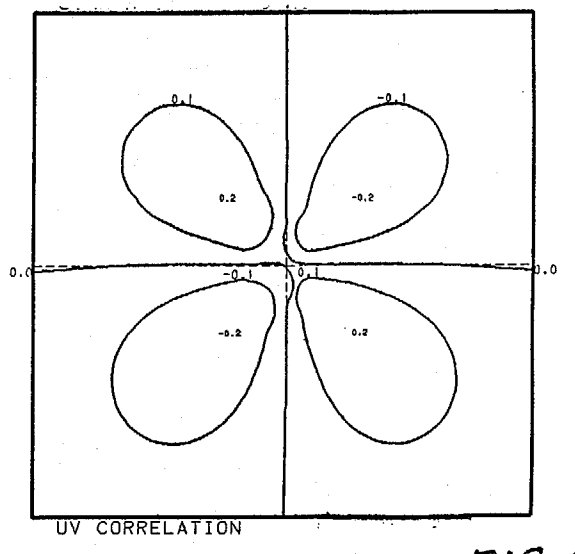
UV CORRELATION

FIG. 1

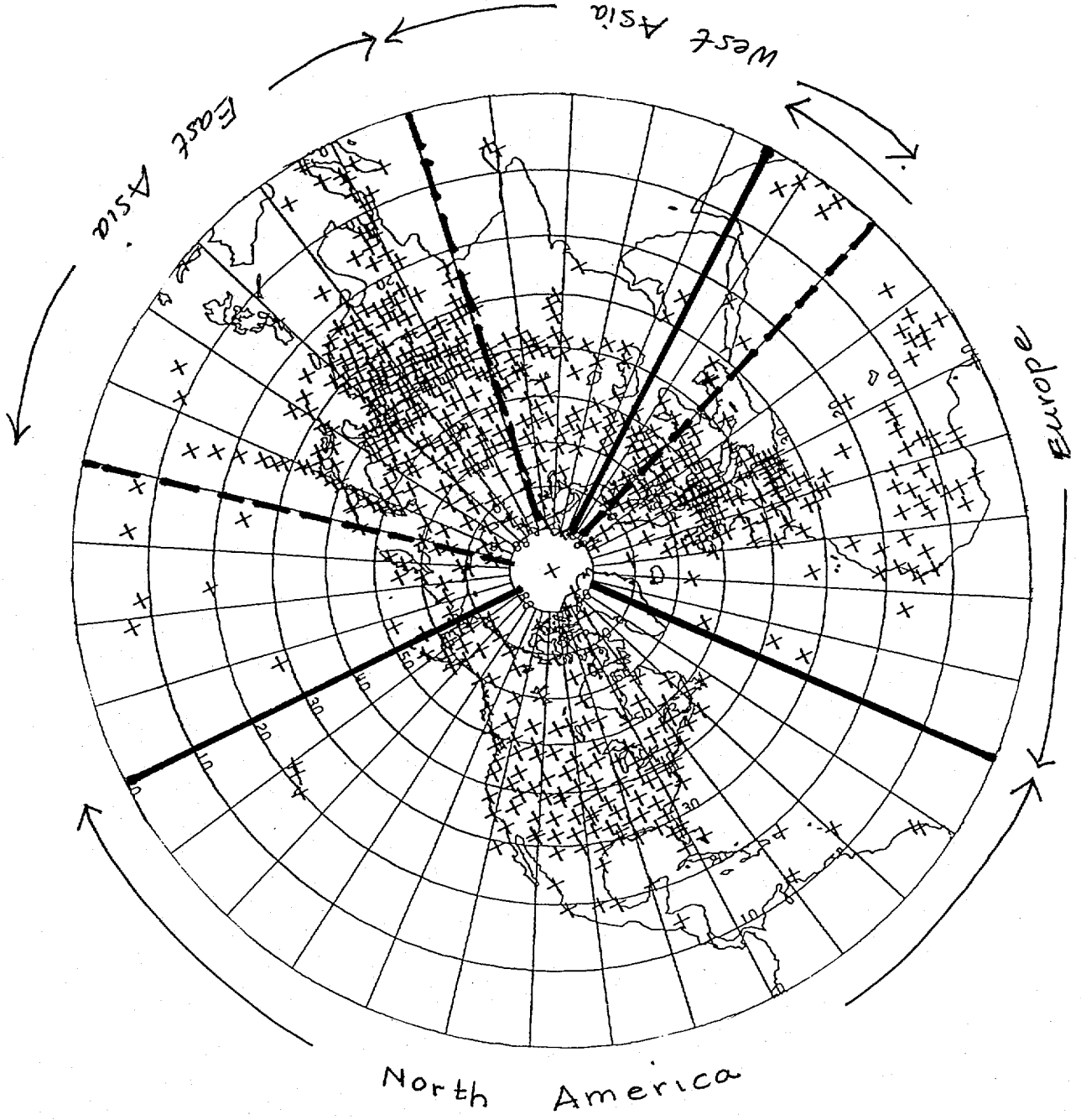

FIG. 2a.

FIGURE 5d

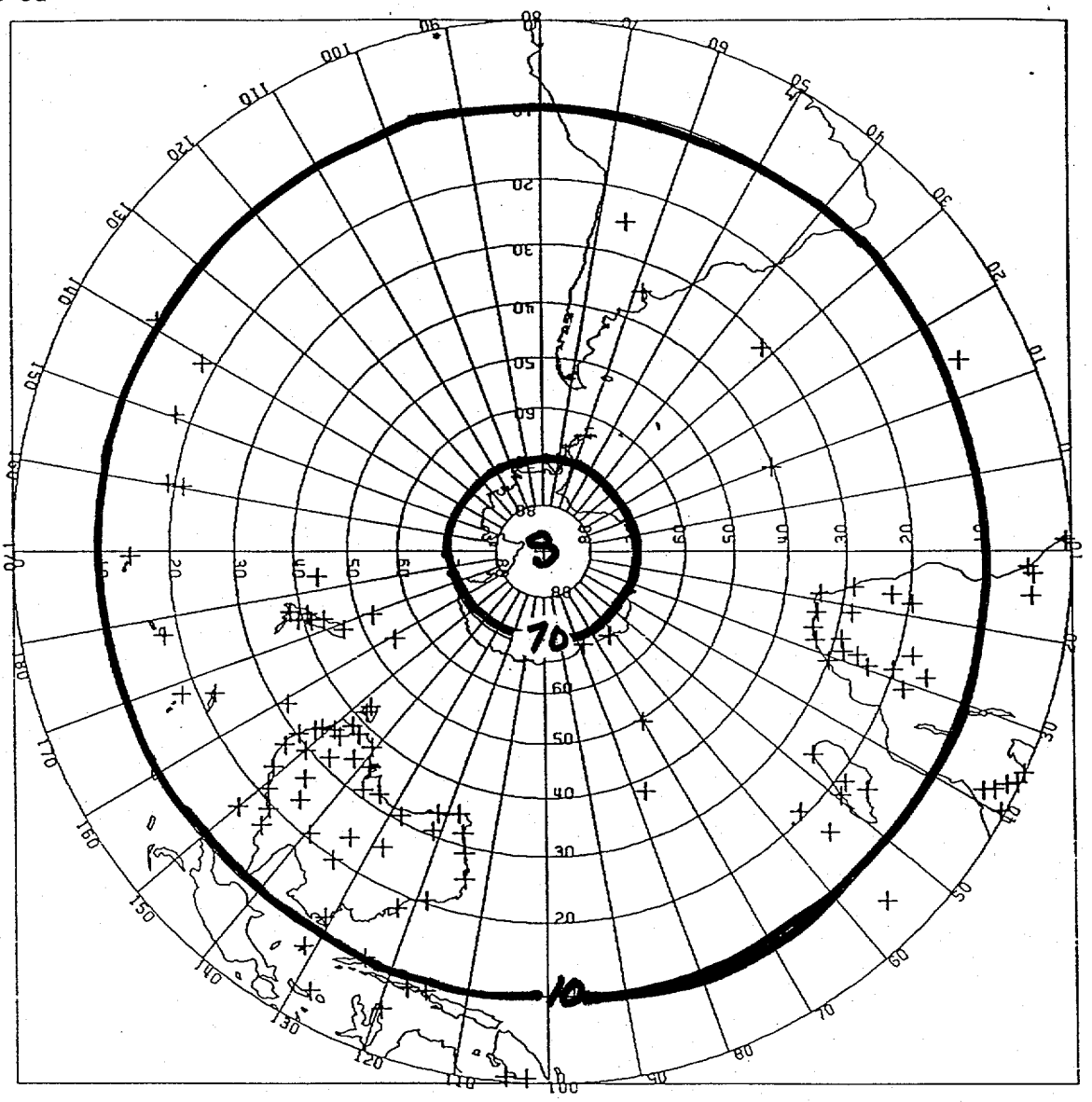

S.H. UPPER AIR OBS. RECEIVED AT NMC WASHINGTON BY 14.23 UCT 87/03/26
DATA COUNT = 109

FIG. 26.

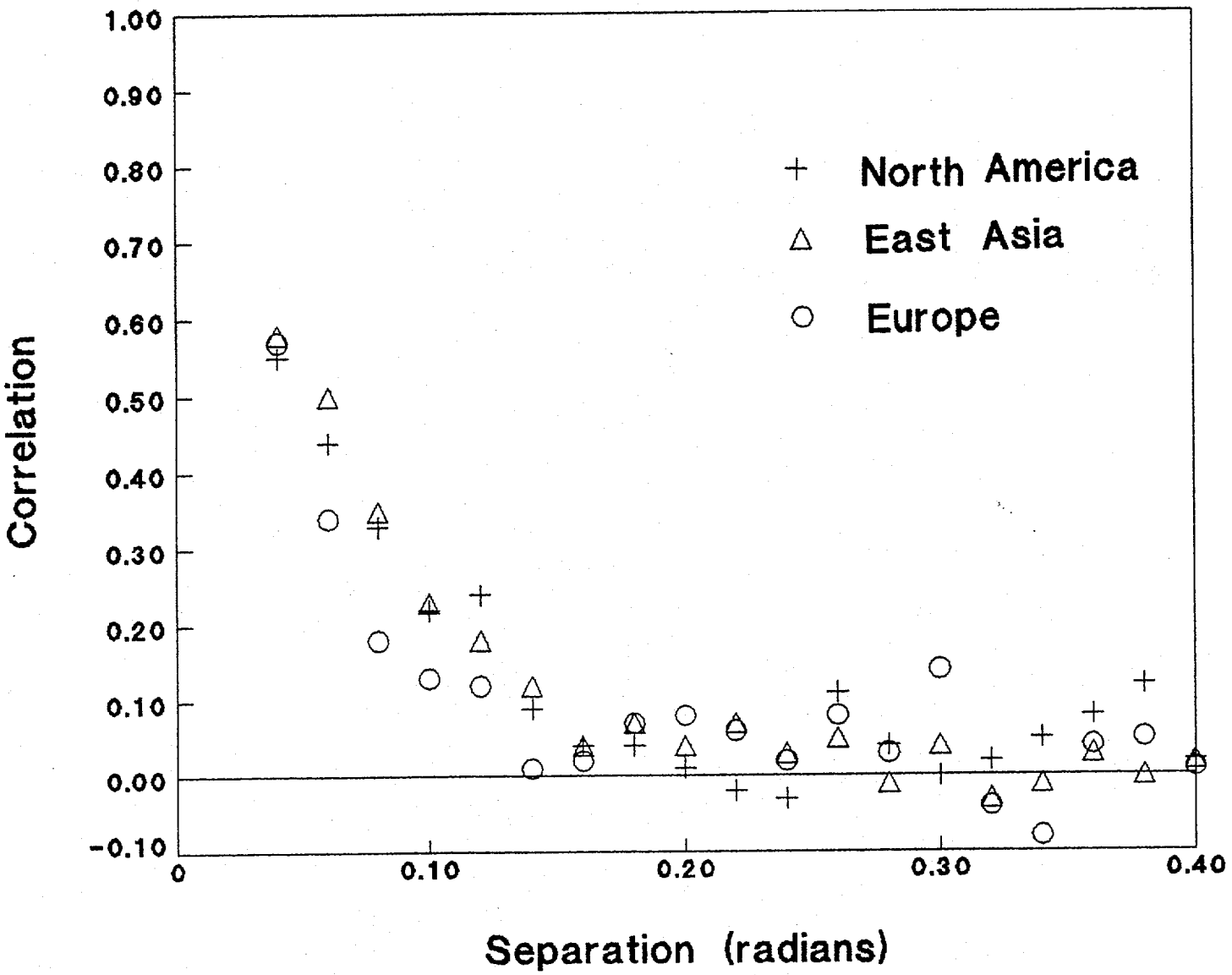
1.00
0.90
0.80
0.70
0.60
0.50
0.40
0.30
0.20
0.10
0.00
-0.10
Correlation
0
0.10
0.20
0.30
0.40
Separation (radians)
North America
East Asia
Europe

Fig. 3.

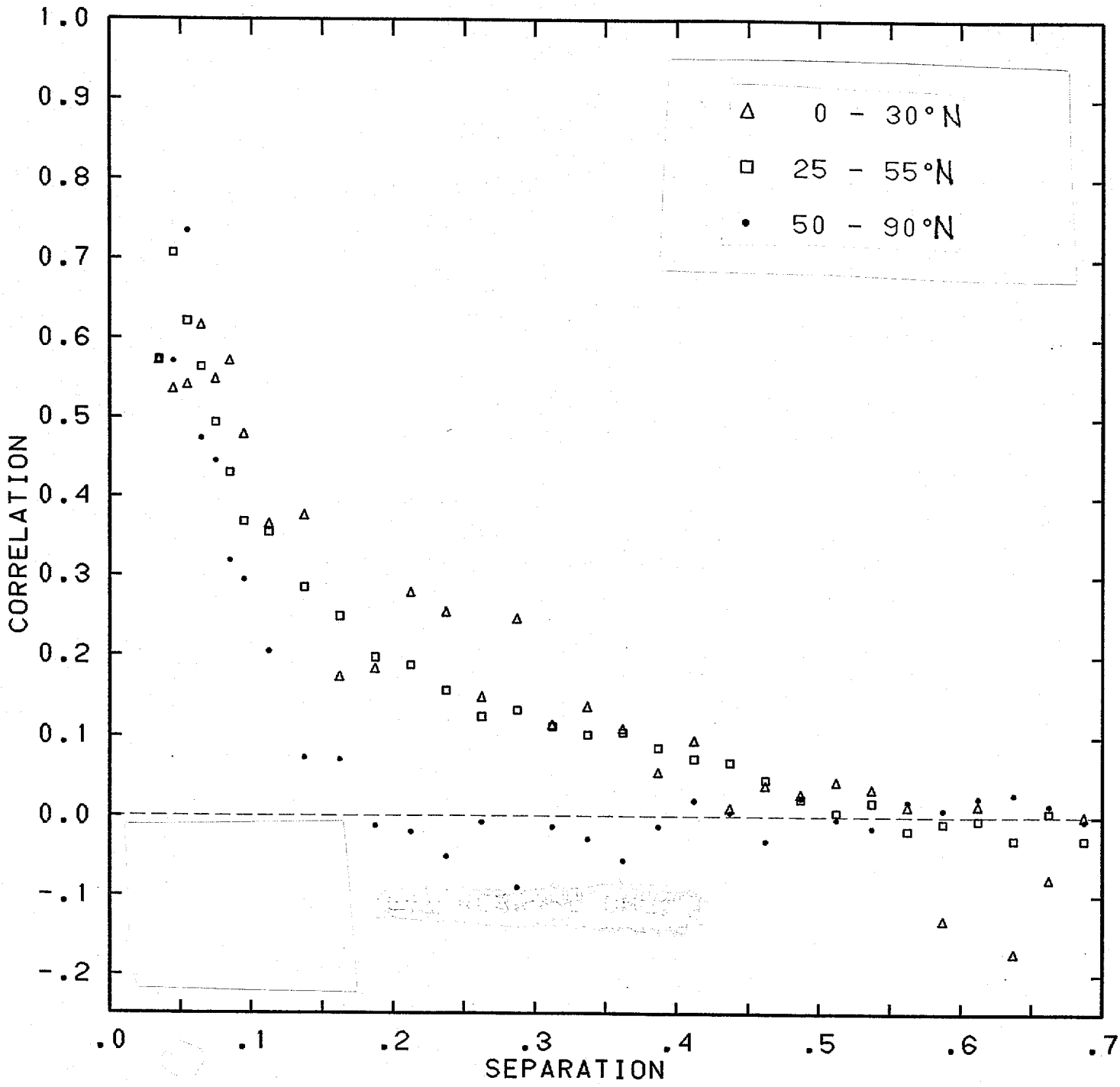
1.0
0.9
0.8
0.7
0.6
0.5
0.4
0.3
0.2
0.1
0.0
-.1
-.2
CORRELATION
.0
.1
.2
.3
.4
.5
.6
.7
SEPARATION
0 - 30°N
25 - 55°N
50 - 90°N

FIG. 5a.

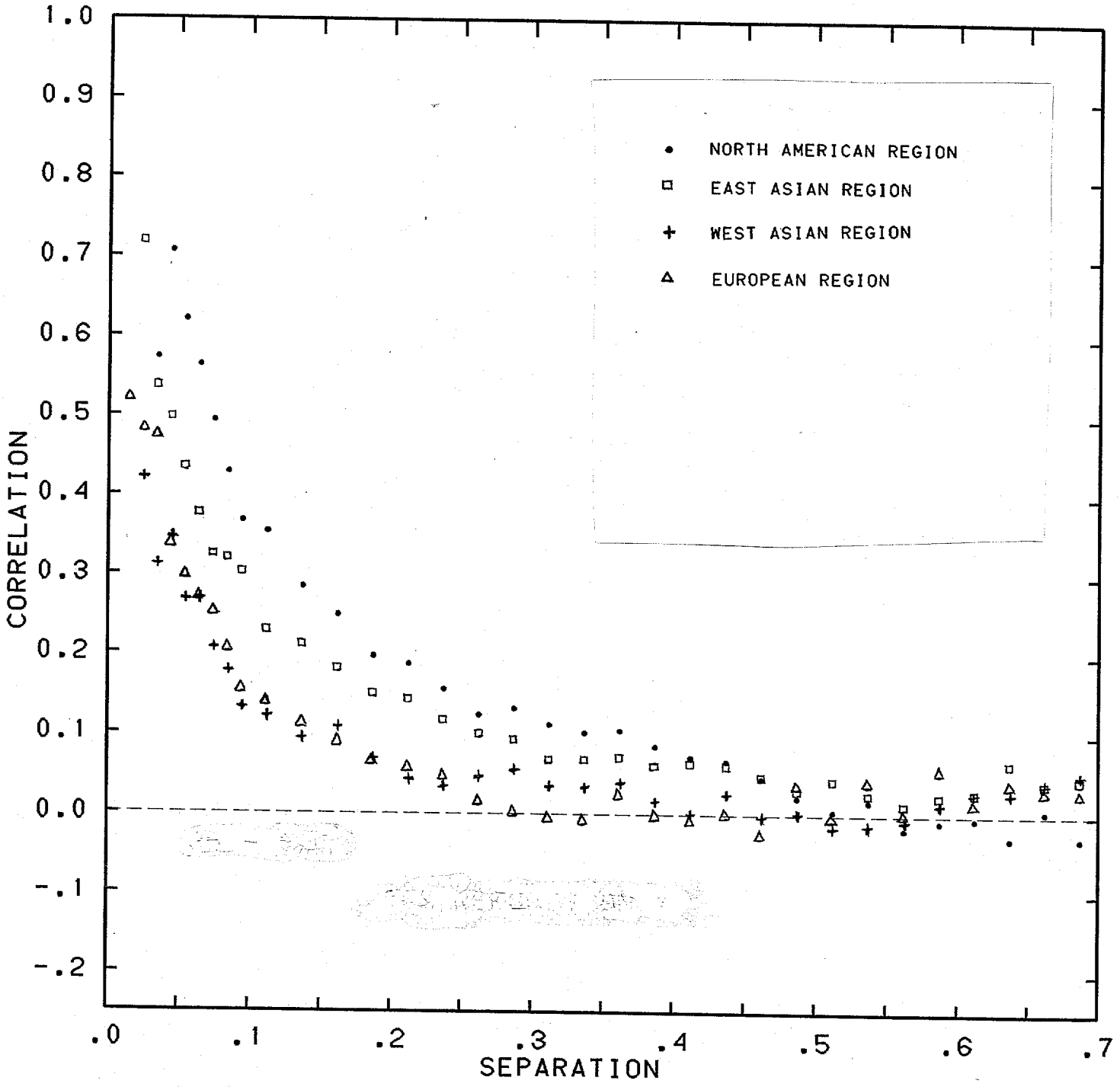
1.0
0.9
0.8
0.7
0.6
0.5
0.4
0.3
0.2
0.1
0.0
-.1
-.2
CORRELATION
.0
.1
.2
.3
.4
.5
.6
.7
SEPARATION
NORTH AMERICAN REGION
EAST ASIAN REGION
WEST ASIAN REGION
EUROPEAN REGION

FIG. 5b.

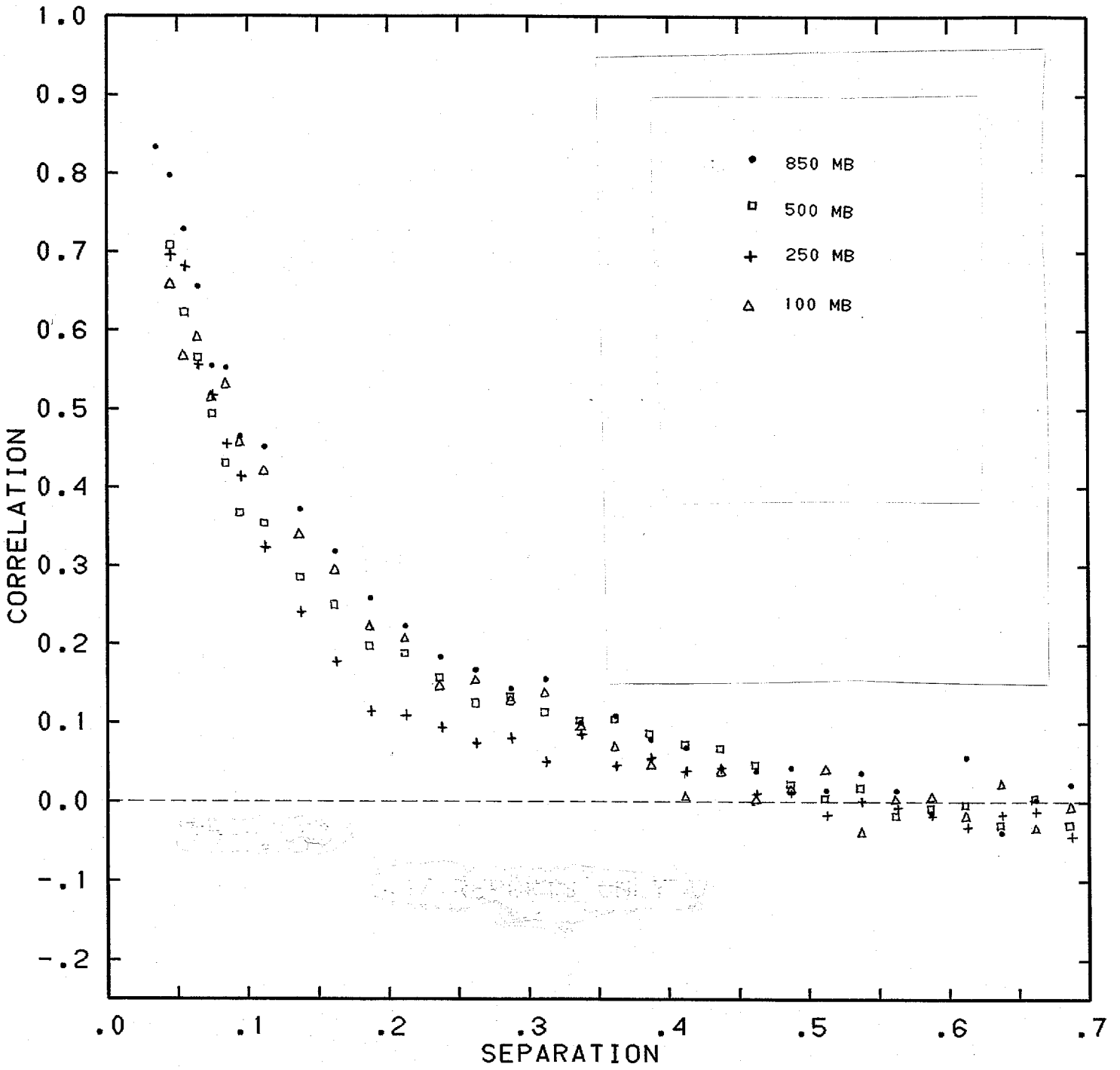
1.0
0.9
0.8
0.7
0.6
0.5
0.4
0.3
0.2
0.1
0.0
-.1
-.2
CORRELATION
.0
.1
.2
.3
.4
.5
.6
.7
SEPARATION
850 MB
500 MB
250 MB
100 MB

FIG. 6

Rankings of Candidates for Geopotential Correlations, based on 1986-87 North American winter f.e.s

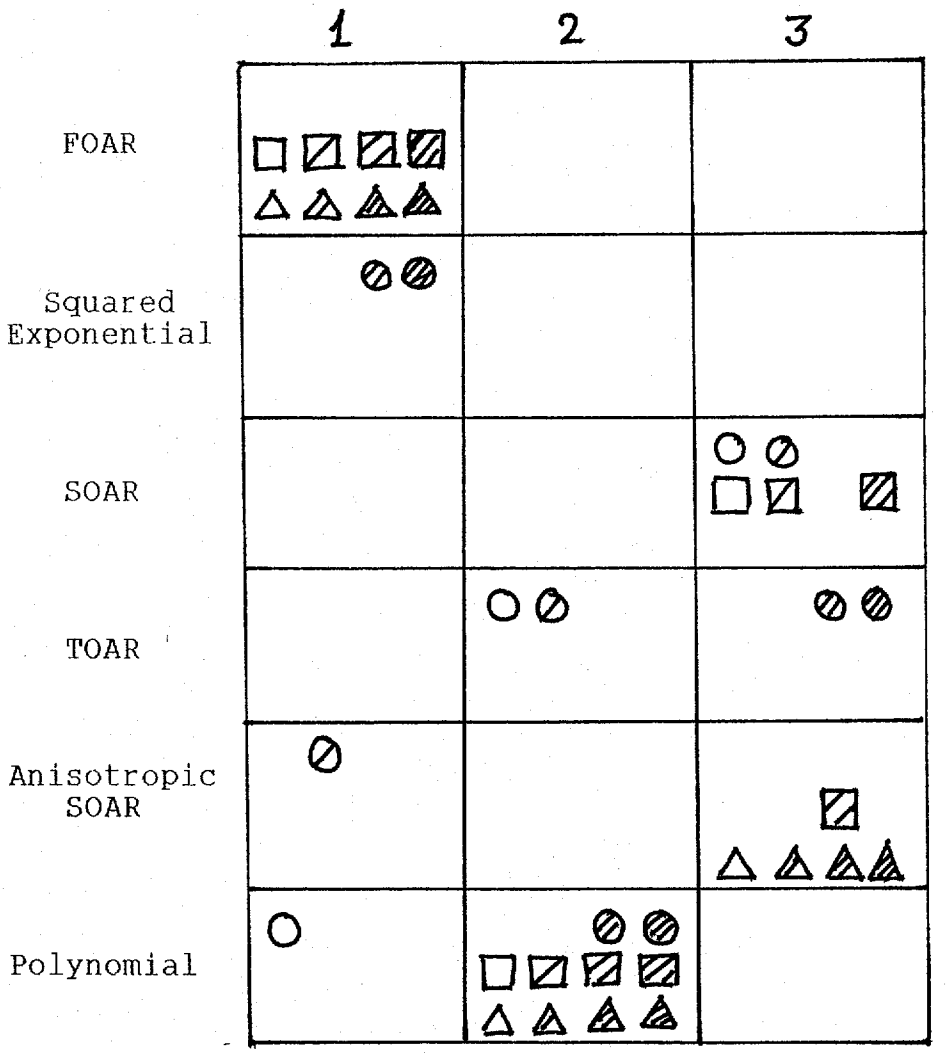

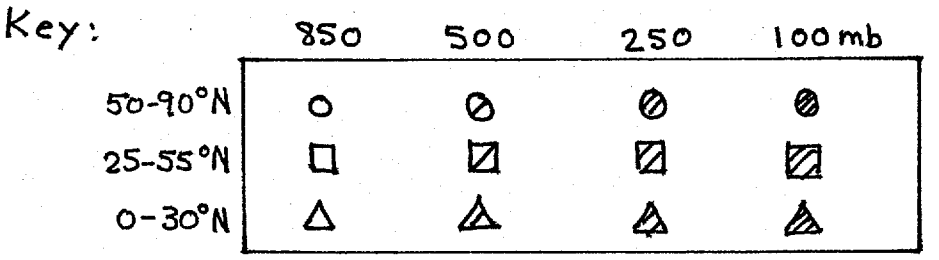

FIG. 7

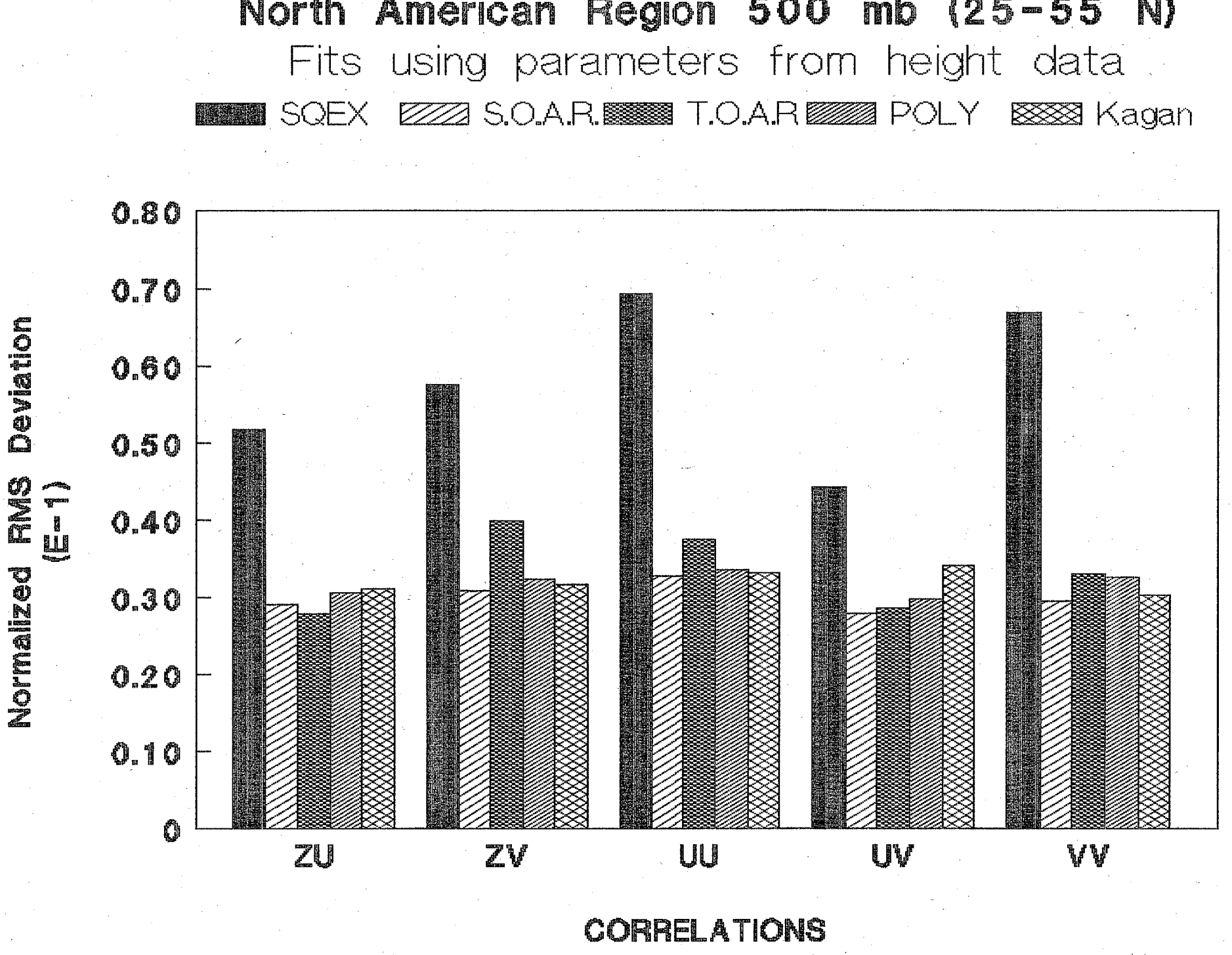
North American Region 500 mb (25-55 N)
Fits using parameters from height data
SQEX
S.O.A.R.
T.O.A.R
POLY
Kagan
Normalized RMS Deviation (E-1)
0.80
0.70
0.60
0.50
0.40
0.30
0.20
0.10
0
ZU
ZV
UU
UV
VV
CORRELATIONS

FIG. 8a

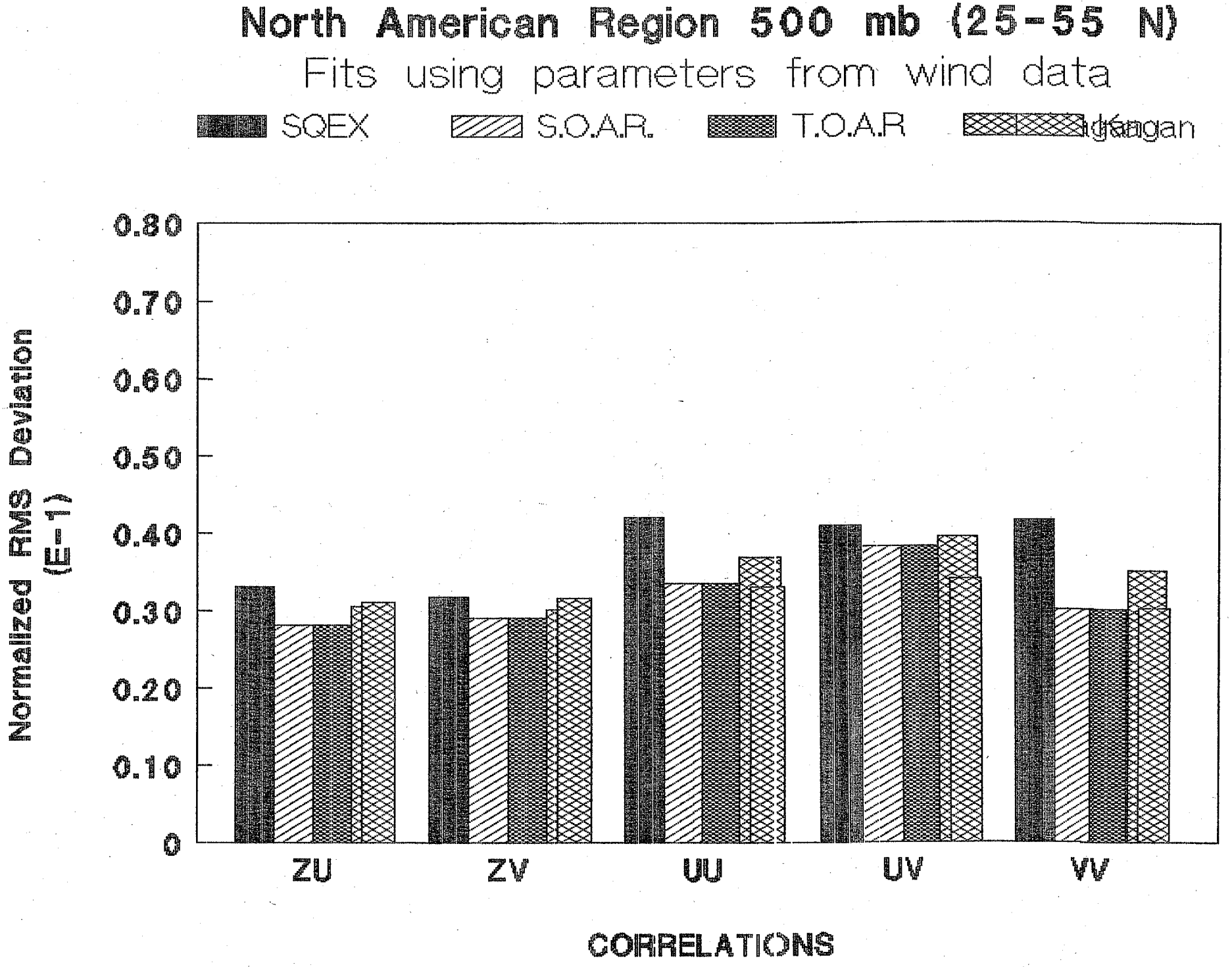
North American Region 500 mb (25-55 N)
Fits using parameters from wind data
SQEX
S.O.A.R.
T.O.A.R
Normalized RMS Deviation (E-1)
0.80
0.70
0.60
0.50
0.40
0.30
0.20
0.10
0
ZU
ZV
UU
UV
VV
CORRELATIONS

FIG. 8b.

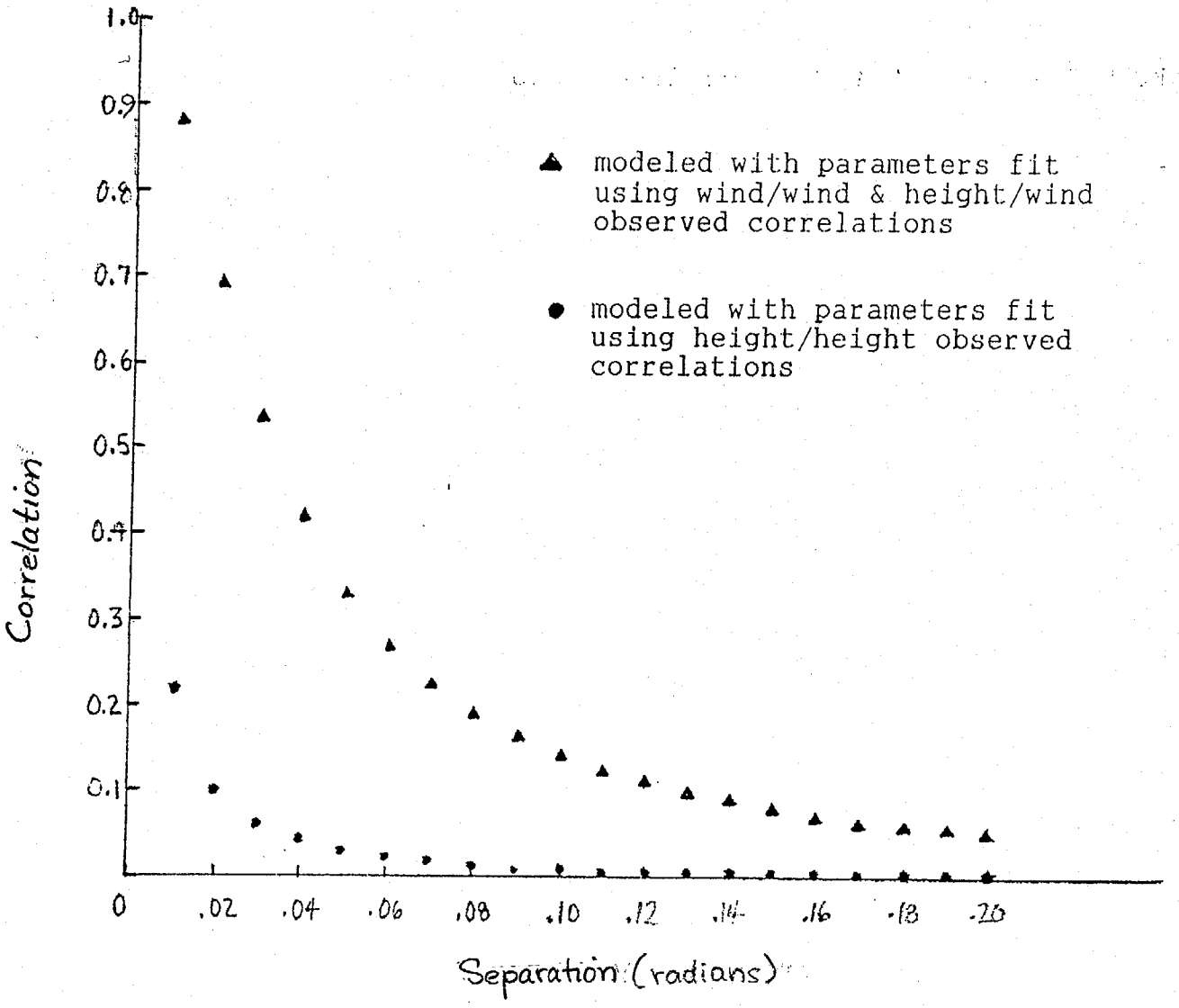
1.0
0.9
0.8
0.7
0.6
0.5
0.4
0.3
0.2
0.1
Correlation
0
.02
.04
.06
.08
.10
.12
.14
.16
.18
.20
Separation (radians)
modeled with parameters fit using wind/wind & height/wind observed correlations
modeled with parameters fit using height/height observed correlations

FIG. 9.

FIGURE CAPTIONS for "Global forecast error correlations"

Figure 1. Contour plots of height/height, height/wind, and wind/wind correlation functions derived from the SOAR basis function. Contours are drawn relative to a single analysis point.

Figure 2.a. Radiosonde station locations for the Northern Hemisphere, shown with regional divisions used in our study. b. As a, for the Southern Hemisphere.

Figure 3. West-to-east cross sections of 500 mb U/U f.e. correlation data for Winter 1986-87 plotted as functions of great circle separation.

Figure 4. Interval averaged 500 mb, winter, geopotential f.e. correlations versus great circle separation in radians. O's denote values computed with 00GMT forecast-minus-RAOB differences and X 's denote values computed with 12GMT data, both for 1986-87. The solid curve was obtained by fitting to 1984-85 f.e. data; and the —·—· curve represents the function currently used by the GDAS.

Figure 5. Interval averaged 500 mb winter geopotential 6-hr f.e. correlations (00GMT) versus great circle separation in radians.
a. compares latitude bands for North America.
b. compares regions defined by longitude between 25 and 55° N latitude.

Figure 6. Comparison of winter, mid-latitude North American Z/Z correlation functions on four isobaric levels: 850, 500, 250, and 100 mb.

Figure 7. Rankings of candidates to represent geopotential f.e. correlation, based on 1986-87 North American winter data, for four pressure levels.

Figure 8. a. Normalized root-mean-square differences between correlation representations derived from four candidate basis functions and the observed auto- and cross-correlation arrays for wind f.e.s, with parameters obtained by fitting the basis function to 500 mb winter geopotential f.e. correlations.
b. As a, but with parameters obtained by simultaneous fitting of the derived wind correlation functions to observed wind correlation arrays.

Figure 9. Comparison of the North American 500mb U/U correlation length scale obtained by fitting to the auto- and cross- correlations of the wind components (Z/U, U/U, U/V, V/V, Z/V) simultaneously, shown as ▲ ▲ ▲, and that obtained by fitting the basis function to the Z/Z correlation array, shown as ● ● ●.